ORIGINAL ARTICLE

Prolonged (>100 Ma) ultrahigh temperature metamorphism in the Napier Complex, East Antarctica: A petrochronological investigation of Earth's hottest crust

Chris Clark[1] | Richard J. M. Taylor[1,2] | Andrew R. C. Kylander-Clark[3] |
Bradley R. Hacker[3]

[1]School of Earth and Planetary Sciences, Curtin University, Perth, WA, Australia

[2]Department of Earth Sciences, University of Cambridge, Cambridge, UK

[3]Department of Earth Science, University of California, Santa Barbara, Santa Barbara, CA, USA

Correspondence
Chris Clark, School of Earth and Planetary Sciences, Curtin University, Perth, WA 6845, Australia.
Email: c.clark@curtin.edu.au

Abstract

The Napier Complex in East Antarctica preserves a record of ultrahigh temperature (UHT) metamorphism during the late Archean to early Palaeoproterozoic. While there is little argument that the UHT metamorphic event began at *c.* 2,580 Ma, the duration over which the rocks resided at UHT has been the subject of intense debate, with estimates for the end of metamorphism ranging from 2,545 to 2,440 Ma—a discrepancy of some 105 Ma. To resolve the time-scale of UHT metamorphism, a zircon and garnet petrochronological (U–Pb, REE and Ti) data set from a suite of rocks from the Tula Mountains region of the Napier Complex was analysed. Individual concordant populations define zircon U–Pb ages for (a) reset zircon cores of 2,502–2,439 Ma; (b) zircon rims of 2,491–2,454 Ma; and (c) neocrystallized sector-zoned zircon from 2,492 to 2,443 Ma. Ti-in-zircon thermometry places a minimum estimate of 830°C for zircon crystallization, with the majority of concordant populations yielding temperatures >900°C. Zircon–garnet partitioning (D_{Yb} vs. $D_{Yb/Gd}$) arrays reveal that the bulk of metamorphic zircon defines an equilibrium relationship with the garnet that forms part of the peak assemblage. Combined with existing geochronological constraints, the new petrochronological data demonstrate that the Napier Complex remained at UHT from *c.* 2,585 Ma until at least 2,450 Ma, a residence time of 135 Ma. In the absence of evidence for contemporaneous emplacement of large volumes of igneous rocks, a number of factors likely combined to drive and maintain these extreme temperatures. We propose that the *P–T* conditions experienced by the Napier Complex were achieved through a combination of orogenic plateau formation, preconditioning of the crust by a high-*T* magmatic and UHT metamorphic event at *c.* 2,850 Ma, inefficient removal of heat-producing elements during partial melting and slow exhumation. This style of long duration, regional, extreme metamorphism is becoming more commonly identified in the rock record as larger and more robust data sets are collected (e.g. the Eastern Ghats of India and the Gondwanan East African Orogen) and is commonly associated with the amalgamation phases of supercontinents/cratons.

KEYWORDS
garnet, hot orogen, long, ultrahigh temperature, zircon

1 | INTRODUCTION

Establishing robust temporal constraints on the thermal evolution of orogenic events is the key to developing an in-depth, quantitative understanding of the processes of mountain building and collapse. There is increasing evidence to suggest that the deep crust of some large orogenic belts may have remained at elevated temperatures (>800°C), where melt is likely to have been present, for long durations (>100 Ma: e.g. Clark et al., 2015; Horton, Hacker, Kylander-Clark, Holder, & Jöns, 2016; Kelsey et al., 2017; Korhonen, Clark, Brown, & Taylor, 2014; Walsh et al., 2015). To accurately gauge how long a terrane has experienced high to ultrahigh temperature, a multi-pronged approach that integrates age and temperature information from accessory minerals with the growth and breakdown of the silicate mineral assemblage needs to be applied. The partitioning of heavy rare earth elements (HREE) between zircon and garnet has long been recognized as the most robust method in evaluating the link between accessory mineral growth and the evolution of the major silicate mineral assemblage during metamorphic events (e.g. Rubatto, 2002). The relationship has been calibrated from natural mineral pairs (Buick, Hermann, Williams, Gibson, & Rubatto, 2006; Hermann & Rubatto, 2003; Hokada & Harley, 2004; Whitehouse & Platt, 2003) and experiments (Rubatto & Hermann, 2007; Taylor, Harley, et al., 2015). A number of studies have demonstrated that the zircon–garnet relationship can withstand long durations of metamorphism at high temperature (Clark, Collins, Santosh, Taylor, & Wade, 2009; Harley & Nandakumar, 2016; Hermann & Rubatto, 2003; Kelly & Harley, 2005; Štípská, Powell, Hacker, Holder, & Kylander-Clark, 2016; Taylor, Clark, Johnson, Santosh, & Collins, 2015), further establishing the utility of zircon–garnet relationships in interrogating the evolution of metamorphic terranes. The recently established ability to rapidly acquire in situ isotopic and trace elemental data sets through techniques such as laser ablation split stream petrochronology means that large coupled geochronological–geochemical data sets can be applied to understanding high-T events (Horton et al., 2016; Kylander-Clark, Hacker, & Cottle, 2013; Shaffer, Hacker, Ratschbacher, & Kylander-Clark, 2017).

The Napier Complex in East Antarctica is probably the most famous UHT terrane, largely because it is the location where the concept of regional UHT metamorphism was first recognized (Dallwitz, 1968; Ellis, 1980; Grew, 1980; Harley, 1998). Despite the early recognition that the UHT metamorphism there affected nearly 100,000 km^2 of crust, the duration of this event(s) remains the subject of ongoing debate. Harley (2016) recently reviewed the evidence for the onset of UHT and suggested—using a combination of in situ U–Pb geochronological and Ti-in-zircon data (Harley, Kinny, Snape, & Black, 2001) and the ages of detrital zircon (Horie, Hokada, Hiroi, Motoyoshi, & Shiraishi, 2012)—that temperatures of >900°C were established by c. 2,580 Ma, and followed by cooling below 900°C at c. 2,500 Ma. By contrast, numerous other studies (e.g. Carson, Ague, & Coath, 2002; Horie et al., 2012) have concluded that the large proportion of metamorphic zircon growth between 2,500 and 2,450 Ma supports the original interpretation of Grew and Manton (1979) that the regional high to ultrahigh temperatures (UHTs) occurred over this time interval.

To resolve these conflicting views, U–Pb zircon geochronology and Ti-in-zircon thermometry has been applied to constrain the timing and conditions of zircon growth for a suite of samples from the Tula Mountains within the Napier Complex. To evaluate the relationship between zircon and garnet growth, we have employed the recently developed rare earth element partitioning array methodology of Taylor et al. (2017) that allows multiple zircon populations to be evaluated visually against different generations of garnet. The combination of data sets allows the duration of metamorphism in the Napier Complex to be more tightly defined. The tighter constraints allow a more robust discussion of the potential drivers of long-lived UHT events and how the Napier Complex fits within the spectrum of UHT metamorphic terrane development through Earth history.

2 | GEOLOGICAL SETTING

The Napier Complex consists of poly-deformed and potentially poly-metamorphosed Archean rocks that crop out along the coast, islands and mountain ranges of Enderby Land in East Antarctica (Figure 1). The rocks within the Napier Complex are dominated by 2,990–2,800 Ma tonalitic to granitic orthogneiss (Black, Williams, & Compston, 1986; Harley & Black, 1987), with interleaved, layered metasedimentary rocks and minor mafic and ultramafic units (Sheraton, Thomson, & Collerson, 1987).

The terrane has experienced at least three deformation events (James & Black, 1981; Sandiford & Wilson, 1983; Sheraton, Tingey, Black, Offe, & Ellis, 1987), some of which are only locally developed (Harley & Black, 1997). During the first deformational event (D$_1$), a regionally sub-horizontal and intensely lineated S$_1$ fabric was developed. This fabric recumbently folds compositional layering and resulted in the transposition and interleaving of the various lithologies. A second deformational event (D$_2$) refolded S$_1$ around tight F$_2$ folds that have inclined to recumbent axial planes; the S$_2$ gneissosity is not pervasive, and only
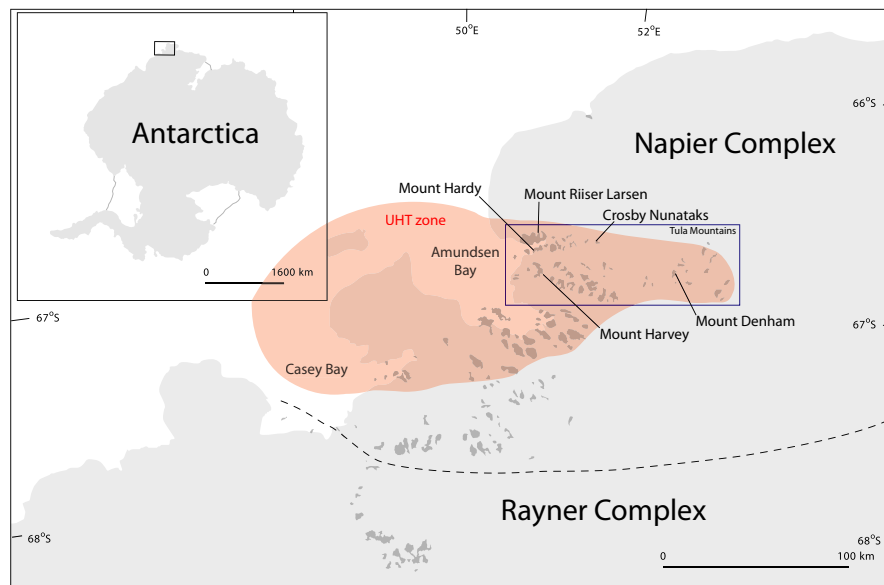
FIGURE 1 Map of the Napier Complex highlighting the area that experienced UHT metamorphic conditions and the Tula Mountains, where samples came from for this study

preserved in rare outcrops (James & Black, 1981). A third deformational event (D_3) resulted in the formation of regional dome-and-basin interference structures with open, upright folds of the earlier fabrics; S_3 is only evident in the hinges of the F_3 folds. The D_1–D_3 structures and associated fabrics are cut by three generations of mafic dykes whose ages range between 2,400 and 1,200 Ma (Sheraton, Tingey, et al., 1987). A suite of amphibolite facies shear zones and pseudotachylites are the final deformational phase; activity on these shear zones has been attributed to reworking during the *c.* 1,000 Ma Rayner event, and 550–500 Ma Pan-African-related reworking (Sandiford, 1985). Carson, Ague, Grove, Coath, and Harrison (2002) dated zircon in these shear zones at 498 ± 1.7 Ma and attributed zircon formation to fluid infiltration.

2.1 | Metamorphic *P–T* evolution of the Napier Complex

The Napier Complex is characterized by the regional occurrence of UHT mineral assemblages that imply peak metamorphic temperatures of 1,050–1,120°C at pressures of 7–11 kbar; the timing of this UHT event has been linked to the generation of the D_1–D_2 structures (Dallwitz, 1968; Ellis, 1980; Grew, 1980; Harley, 1998; Hokada, 2001; Hokada & Harley, 2004; Hokada, Motoyoshi, Suzuki, Ishikawa, & Ishizuka, 2008; Motoyoshi, Hensen, & Matsueda, 1990; Sandiford, 1985; Sheraton, Tingey, et al., 1987). The highest temperatures are restricted to a central part of the Napier Complex (Kelly & Harley, 2005). UHT metamorphism in the Napier Complex was followed by a period of isobaric cooling (IBC) at pressures of <8 kbar in the northern parts of the Complex (Amundsen Bay and Tula Mountains) and at pressures of ~9–10 kbar in areas farther south (Kelly & Harley, 2005 and

references therein). Hollis and Harley (2002) reported evidence for 1–3 kbar of isothermal decompression at temperatures greater than 1,000°C, prior to IBC in the UHT region. Shimizu, Tsunogae, and Santosh (2013) presented evidence that two different styles of UHT metamorphism can be observed: a suite of rocks from Tonagh Island in the west have near-IBC paths, whereas rocks to the east at Priestly Peak display evidence for up to 5 kbar of post-peak decompression from a peak pressure of 12 kbar. They concluded that these two areas may have undergone different tectonic histories as a result of their different positions within a subduction/collisional system. The varying styles of post-peak exhumation across the Napier Complex proposed in the studies of Shimizu et al. (2013) and Hollis and Harley (2002)—and the many studies that report only IBC trajectories—are consistent with the observed field pressure gradient proposed by Harley and Hensen (1990) and refined by Hokada et al. (2008). Hokada et al. (2008) proposed that the observed 4 kbar of pressure variation from north to south across the UHT zone is a result of juxtaposition of different crustal blocks by vertical movement along shear zones. While there seems to be a significant variation in the crustal levels of exposed rocks, the temperatures within the different blocks all record peak metamorphic temperatures in excess of 1,000°C.

2.2 | Age constraints on metamorphism of the Napier Complex

As outlined above, the timing of metamorphism and deformation within the Napier Complex has been, and continues to be, the subject of ongoing debate. Early workers in the terrane inferred a *c.* 3,000 Ma age for metamorphism based on Rb–Sr isochrons and zircon upper-intercept ages (James & Black, 1981). Grew and Manton (1979) suggested that peak

metamorphism occurred in the Napier Complex at *c.* 2,500 Ma based on ages from synmetamorphic charnockitic pegmatites. James and Black (1981) reasoned that the zircon ages that cluster near *c.* 2500 Ma reflect resetting associated with D_3 retrograde amphibolite–granulite grade metamorphism. A number of subsequent studies have found abundant evidence of metamorphic zircon growth in the age range 2,500–2,450 Ma (Asami, Suzuki, & Grew, 2002; Black, 1988; Black, James, & Harley, 1983a, 1983b; Black, Sheraton, & James, 1986; Black, Williams, et al., 1986; Carson, Ague, & Coath, 2002; Carson, Ague, Grove, et al., 2002; Grew, Suzuki, & Asami, 2001; Harley & Black, 1997; Hokada et al., 2008; Horie et al., 2012; Kelly & Harley, 2005; Shiraishi et al., 1997) that support the original suggestion of Grew and Manton (1979) and Grew (1982) that peak UHT metamorphism occurred at this time. By contrast, Harley et al. (2001) proposed that the 2,500–2,450 Ma zircon ages record not UHT metamorphism, but post-peak zircon formation, diffusional Pb loss or a combination of these processes. They advocated an age range of 2,590–2,550 Ma for the UHT event based on REE relationships between zircon and garnet from discordant leucosomes. Kelly and Harley (2005) extended the minimum age estimate of UHT metamorphism down to 2,510 Ma based on the REE characteristics of zircon and garnet pairs—although they preferred a lower limit of 2,545 Ma. Most recently, Harley (2016) presented evidence from zircon U–Pb and Ti-in-zircon thermometry from McIntyre Island in the southern part of the Napier Complex—combined with the study of Hokada and Harley (2004)—that extends the duration of metamorphism to 2,500 Ma. Following the UHT event, slow cooling at ~2–3 °C/Ma over 40–100 Ma is suggested by Sm–Nd and Lu–Hf whole-rock isochrons of 2,380–2,360 Ma and 2,400 Ma respectively (Choi et al., 2006; Suzuki, Arima, Williams, Shiraishi, & Kagami, 2006).

There is evidence for a low-*P*, high-*T* metamorphic/magmatic event throughout the Napier Complex at *c.* 2,850 Ma prior to the UHT event at *c.* 2,500 Ma (Kelly & Harley, 2005; Kusiak, Whitehouse, Wilde, Nemchin, & Clark, 2013). However, the precise timing of peak metamorphism, and the duration of this event and its synchronicity across the Napier Complex is still poorly resolved (e.g. Harley & Black, 1987) due to the extreme nature of the subsequent overprinting UHT event.

3 | METHODS

3.1 | Laser ablation split stream inductively coupled plasma mass spectrometry

Data were collected during a long session of standards (*n* = 904) as well as Proterozoic and Archean unknowns (*n* = 1,030). Instrumentation consists of a Photon Machines Analyte 193ArF laser ablation system coupled to an Agilent 7700x quadrupole ICP and a Nu Instruments Plasma HR MC-ICPMS at the University of California, Santa Barbara (UCSB). The Analyte 193 is based on an ATLEX SI ArF 193 nm wavelength excimer laser, equipped with a low-volume HeLeX sample cell (Photon Machines, San Diego, CA, USA) modified from the design of Eggins, Rudnick, and McDonough (1998). Operating conditions for the instrument were routine (e.g. Cottle, Kylander-Clark, & Vrijmoed, 2012; Kylander-Clark et al., 2013), with a 30 μm ablation spot size, a fluence of ~2.5 J/cm² and a repetition rate of 4 Hz, which ablates at a rate of ~0.1 μm per pulse. Data acquisition consists of two laser pulses at the start of measurement to remove surface contamination, a 15-s washout period during which the background signal is collected, 25 s of continuous ablation during which data are collected and ~3 s with no laser firing to allow dispersal of all sample material before the next analysis. The ablated material is carried by He from the sample cell and then mixed with Ar to stabilize the aerosol before input to the plasma. Immediately after mixing, the ablation stream is split into approximately half and directed into each mass spectrometer.

U–Th–Pb isotope data were collected using a Nu-Plasma high-resolution multicollector ICPMS (Nu Instruments, Wrexham, UK) which consists of 12 Faraday cups and four ETP discrete dynode electron multipliers. The detection system on the Nu-Plasma at UCSB allows for simultaneous measurement of ^{208}Pb, ^{207}Pb ^{206}Pb, ^{232}Th and ^{238}U on Faraday cups equipped with 10^{11} ohm resistors and ^{204}Pb+Hg and ^{202}Hg on two ETP discrete dynode electron multipliers. A sample-standard bracket approach was used, with BR266 zircon (559 Ma; Stern & Amelin, 2003) used as the primary reference material to monitor and correct for mass fractionation and instrumental drift. Secondary reference zircon GJ1 (601 Ma; Jackson, Pearson, Griffin, & Belousova, 2004), Plešovice (337 Ma; Sláma et al., 2008), 91500 (1,060 Ma; Wiedenbeck et al., 2004) and OG1 (3,465 Ma; Stern, Bodorkos, Kamo, Hickman, & Corfu, 2009) were used to monitor data accuracy and precision, and were corrected for mass bias and fractionation based on measured isotopic ratios of the primary reference material. The accuracy of $^{207}Pb/^{206}Pb$ ratios was verified by comparison with the Archean OGC-1 zircon standard. A typical analytical run consisted of ~90 min with ~115 analyses of unknowns and standards. The time-resolved mass spectra were reduced using the U_Pb_Geochronology4 data reduction scheme in Iolite (Paton, Hellstrom, Paul, Woodhead, & Hergt, 2011 and references therein). Continued analysis of Archean secondary standard OG1 provided the most appropriate representation of unknowns and was used to calculate an additional uncertainty on top of the analytical uncertainty propagated through all unknowns. This additional uncertainty was

+1.5% on $^{206}Pb/^{238}U$ errors and +0.8% on $^{207}Pb/^{206}Pb$ errors. The secondary reference materials yielded within uncertainty of published ages, with accuracy of $^{206}Pb/^{238}U$ weighted mean ages within 0.5 % of accepted values 599 ± 0.7 Ma for GJ1 (MSWD = 1.4, n = 229 of 236), 336 ± 0.4 Ma for Plešovice (MSWD = 1.17, n = 102 of 108) and 1,056 ± 2.8 Ma for 91500 (MSWD = 1.2, n = 147 of 150). The OG1 reference material yielded a $^{206}Pb/^{238}U$ weighted mean age of 3,464 ± 4 Ma (MSWD = 1, n = 152 of 159) and a $^{207}Pb/^{206}Pb$ weighted mean age of 3,458 ± 4 Ma (MSWD = 1, n = 151 of 159).

Trace element concentrations were measured simultaneously on an Agilent 7700x quadrupole ICP-MS. GJ1 zircon was used as calibration standard to monitor and correct for mass fractionation and instrumental drift. Data were collected using time-resolved data acquisition and processed using the Iolite software package (Paton et al., 2010, 2011). Where appropriate, REE values were normalized to chondritic values (Anders & Grevesse, 1989). GJ1 was run every 8–10 unknowns per sample, with three analyses at the beginning and end of each run. Stoichiometric major elements were used for calibration of trace elements in each phase. Internal standardization was done stoichiometrically assuming 100% $ZrSiO_4$ (i.e. 43.14 % Zr). Measured elements were ^{27}Al, ^{29}Si, ^{31}P, ^{44}Ca, ^{49}Ti, ^{89}Y, ^{90}Zr, ^{139}La, ^{140}Ce, ^{141}Pr, ^{146}Nd, ^{147}Sm, ^{153}Eu, ^{157}Gd, ^{159}Tb, ^{163}Dy, ^{165}Ho, ^{166}Er, ^{169}Tm, ^{172}Yb, ^{176}Lu and ^{179}Hf. Uncertainties on individual spot measurements are cited at 2σ level and include the internal uncertainties associated with counting statistics only.

3.2 | LA-ICP-MS garnet

Rare earth element and other trace element compositions of garnet were measured using LA-ICP-MS, using an ASI Resolution M-50 193-nm wavelength ArF excimer laser with an Agilent 7700 mass spectrometer at Curtin University. Garnet grains were analysed in thin section using a 50 μm spot size. The ablation period was 30 s with a repetition rate of 7 Hz. NIST glasses (610, 612; Pearce et al., 1997) were used as reference materials. NIST 610 was used as the primary standard for garnet. Stoichiometric major element compositions were used for calibration of trace elements in garnet (Si = 18 wt%). Time-resolved data were processed following each session using the Iolite software (Paton et al., 2010, 2011), also allowing the detection and elimination of data affected by analysing inclusions. In the REE plots, the analysed data are normalized against the chondrite values of Anders and Grevesse (1989).

3.3 | Ti-in-zircon thermometry

The Ti content of zircon coexisting with rutile and quartz has a strong dependence on temperature, and this dependence

has been calibrated as a thermometer (Watson & Harrison, 2005) and applied to UHT rocks (e.g. Baldwin, Brown, & Schmitz, 2007; Korhonen et al., 2014; Shaffer et al., 2017). This thermometer was applied to the eight samples from the Tula Mountains, using the calibration for Ti-in-zircon of Ferry and Watson (2007). For Ti-in-zircon thermometry, rather than simply taking the highest temperature determined from each data set, we follow the proposal by Tomkins, Powell, and Ellis (2007) and use a conservative estimate of temperature as given by the upper bound of a box plot box. These authors suggested the uncertainty associated with this value be approximated as ±30°C or half the interquartile range if this is larger, based on the rationale that the real uncertainty relates to the scatter in the data rather than to analytical uncertainties combined with calibration uncertainties, which are likely to be much smaller than ±30°C.

4 | SAMPLE DESCRIPTIONS

The samples used in the study were collected during the 1977/1978 and 1979/1980 Australian National Antarctic Research Expeditions to Enderby Land (Figure 1). A range of lithologies and locations were chosen for analysis based on their suitability for petrochronological investigation. The main mineral assemblages and cathodoluminescence (CL) characteristics of zircon grains are summarized in Table 1 and key features of the rocks are illustrated in Figures 2a–p and 3a–h.

4.1 | Mount Riiser Larsen

91279-14 is dominated by an assemblage of coarse-grained garnet (Grt 1), orthopyroxene (Opx), mesoperthite (Fsp) and quartz (Qz) (Figure 2a). The coarse-grained quartz (Qz(Rt)) contains abundant rutile needles whose orientations appear to be crystallographically controlled (Figure 2b). Coarse-grained garnet is mantled by a second generation of garnet (Grt 2) that is intergrown with quartz (Figure 2a). CL imaging of zircon grains identified a variety of textures with a range of CL responses (Figure 3a). A population of grains is characterized by oscillatory-zoned cores with high-CL response typical of zircon grown in a magmatic environment (Ch); other grains show irregular zonation or broad featureless zones with low-CL response (Cl). Core domains have overgrowths of either high (Rh) or low (Rl) CL response. Two generations of neocrystallized, sector-zoned grains are also present with both CL high (Sh) and CL low (Sl) varieties.

4.2 | Crosby Nunataks

Sample 171279-1 contains a coarse-grained assemblage of orthopyroxene (Opx 1), quartz with rutile exsolution

TABLE 1 Summary of petrochronological data from the Tula Mountains

Sample	Mineralogy	Zircon CL[a]	Concordia age[b] Ma ± 2s (MSWD[c], n[d])	Ti-in-Zrc T[e] (°C, ±30)	Zircon chemistry Yb$_n$/Gd$_n$	Th/U	Garnet Type	Yb$_n$/Gd$_n$	Eu/Eu*
Mount Riiser Larsen									
91279-14	Grt–Opx–Fsp–Qz(Rt)[f]–Ilm	Ch	2,439 ± 14 (1.40, 3)	894	2.02–2.25	0.14–0.43	Grt 1	7.96–9.94	0.44–0.47
		Cl	2,505–2,434 (11)	904	4.25–43.77	0.02–0.20	Grt 2	6.58–7.97	0.49–0.56
		Rh	2,460 ± 11 (2.00, 21)	909	0.63–7.13	0.16–1.33			
		Rl	2,470 ± 16 (0.96, 2)	932	4.13–6.10	1.60–1.67			
		Sh	2,455 ± 11 (0.61, 6)	919	2.09–13.97	0.23–0.82			
		Sl	2,443 ± 14 (1.90, 2)	847	4.69–7.25	0.14–0.65			
Crosby Nunataks									
171279-1	Opx–Osm–Qz(Rt)–Spr–Crd–Fsp	Ch	2,844–2,502 (12)	895	1.09–86.72	0.02–2.89			
		Cl	2,833–2,480 (9)	897	1.18–26.19	0.03–2.78			
		Rh	2,475 ± 15 (1.02, 4)	858	1.83–6.90	1.71–2.34			
		Rl	2,490 ± 10 (0.61, 10)	879	1.25–11.56	0.02–2.37			
171279-3	Grt–Osm–Qz(Rt)–Fsp–Crd–Opx	Ch	2,849–2,457 (42)	904	0.67–21.67	0.34–0.86	Grt 1	0.18–0.63	0.55–1.27
		Cl	2,457 ± 33 (3.5, 3)	871	1.56–4.01	0.12–0.77	Grt 2	0.96–1.96	0.60–0.82
		Rh	2,454 ± 9 (2.00, 8)	904	1.39–5.41	0.67–1.01	Grt 3	1.29–1.84	0.54–0.65
171279-9	Opx–Grt–Fsp–Qz(Rt)–Ilm	Ch	2,502 ± 24 (2.8, 5)	905	5.65–14.42	0.07–0.44	Grt 1	19.28–39.12	−0.13 to 0.19
		Cl	2,691–2,427 (10)	904	6.63–75.07	0.02–0.62	Grt 2	7.90–17.89	−0.02 to 0.11
		Rh	2,470 ± 13 (1.04, 5)	918	8.68–9.61	0.20–0.74			
		Rl	2,491 ± 12 (0.50, 6)	906	7.58–18.54	0.03–0.47			
		Sh	2,474 ± 21 (0.76, 2)	914	5.10–10.38	0.13–0.67			
171279-10	Opx–Fsp–Qz(Rt)–Ilm	Ch	2,858–2,486 (46)	943	11.14–39.36	0.41–0.84			
		Cl	2,596–2,513 (6)	952	42.12–186.73	0.14–0.35			
		Rh	2,483 ± 16 (2.50, 3)	856	19.76–159.25	0.23–1.84			
Mount Hardy									
91279-13	Grt–Opx–Fsp–Qz(Rt)–Spr–Spl–Rt–Crd	Cl	2,665–2,352 (2)	863	4.35–19.46	0.02–0.52	Grt 1	0.15–0.52	0.37–0.44
		Sl	2,492 ± 7 (0.48, 19)	915	9.93–17.52	0.10–0.38	Grt 2	0.04–0.23	0.57–0.88
Mount Harvey									
3180-2	Grt–Sill–Qz(Rt)–Rt–Fsp	Ch	2,784–2,475 (2)	989	1.63–19.46	0.60–1.03	Grt 1	0.73–0.84	0.12–0.23
		Cl	3,281–2,519 (2)	946	16.50–102.44	0.03–0.45			
		Sh	2,454 ± 11 (1.70, 6)	915	0.63–2.89	0.89–1.24			
		Sl	2,461 ± 7 (1.30, 19)	899	0.27–4.44	0.11–1.61			
Denham Peak									
3180-7	Grt–Opx–Qz(Rt)–Fsp	Cl	2,609–2,431 (25)	843	5.79–95.32	0.02–0.50	Grt 1	3.16–3.43	0.07–0.17
		Rl	2,471 ± 7 (1.60, 28)	837	0.37–5.48	0.04–0.17			
		Sl	2,474 ± 5 (0.87, 9)	828	0.56–6.97	0.04–0.12			

[a]Cathodoluminescence (CL) texture: Ch, core high response; Cl, core low response; Rh, rim high response; Rl, rim low response; Sh, sector-zoned high response; Sl, sector-zoned low response.

[b]Concordia age as defined by Ludwig (1998) calculated for $^{207}Pb/^{206}Pb$–$^{238}U/^{206}Pb$ pairs. Where no age was calculated, the range of concordant dates is presented.

[c]MSWD of concordance and equivalence.

[d]n is the number of analyses used in the calculation of the concordia age.

[e]Ti-in-Zrc temperatures calculated using the calibration of Ferry and Watson (2007) using the upper bound of the box plot as per Tomkins et al. (2007).

[f]Qz(Rt): quartz contains crystallographically controlled rutile lamellae.
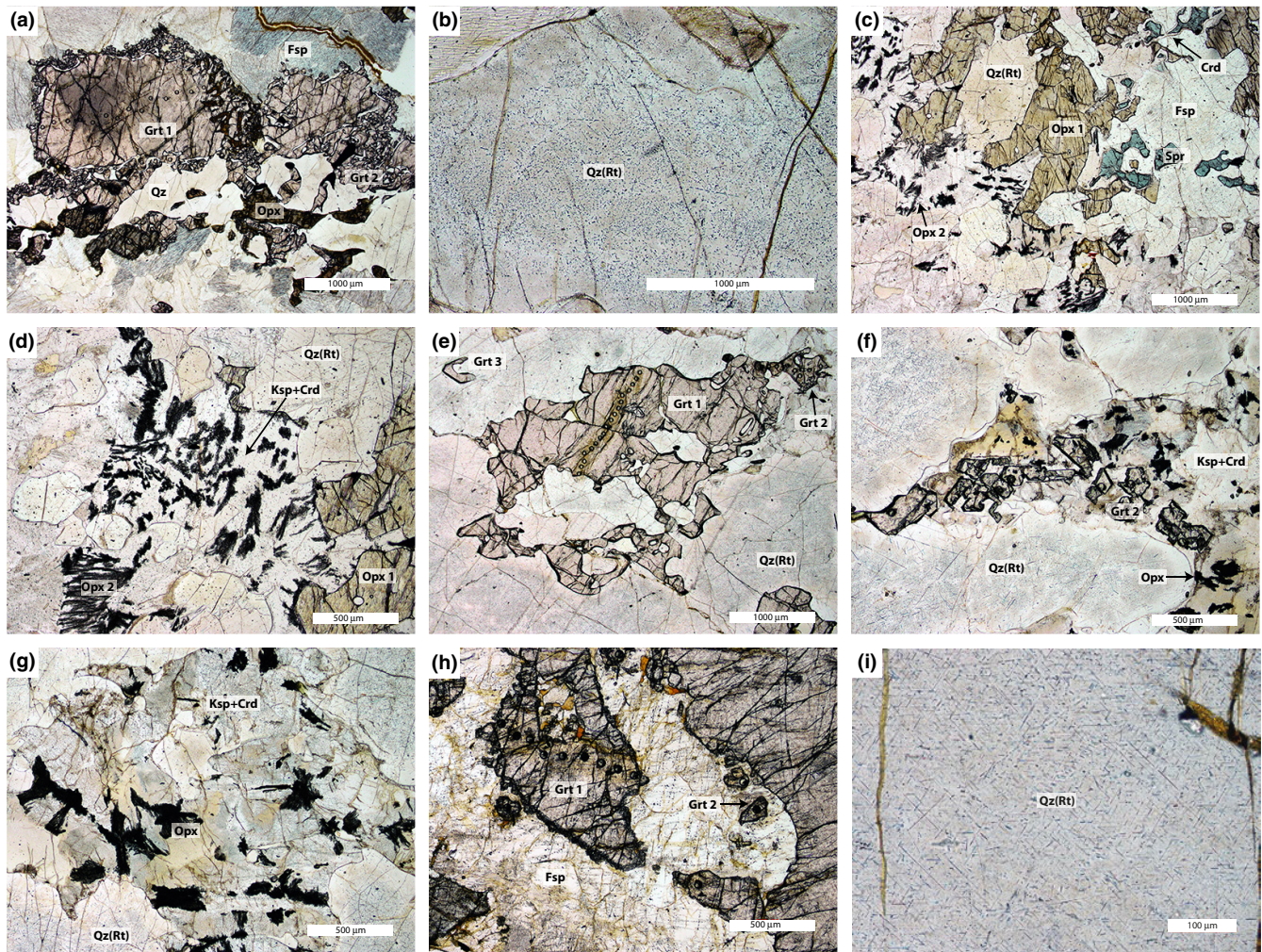
* = geochemical measure.

FIGURE 2 (a–p) Photomicrographs of key petrographic relationships from samples within this study. The reader is referred to the main text for the description of the photomicrographs

lamellae (Qz(Rt)), mesoperthite (Fsp) and sapphirine (Spr) (Figure 2c). Sapphirine is observed in textural equilibrium with orthopyroxene and quartz, suggesting that this rock experienced temperatures >900°C. Sapphirine is locally separated from quartz by a thin corona of cordierite (Figure 2c). Isolated intergrowths of K-feldspar (Ksp), cordierite, quartz and fine-grained dendritic orthopyroxene (Opx 2) distributed throughout the rock are interpreted to have formed via the breakdown of peak osumilite (e.g. Ellis, Sheraton, England, & Dallwitz, 1980; Figure 2d). Zircon grains display both oscillatory-zoned high (Ch) and low CL (Cl) response and are mantled by CL low (Rl) and high (Rh) rims that are the result of recrystallization of the pre-existing zircon cores (Figure 3b).

Sample 171279-3 (previously reported in Taylor et al., 2017) is a quartz-rich rock containing coarse-grained garnet (Grt 1) and quartz with abundant rutile exsolution lamellae (Qz(Rt)) (Figure 2e). A second textural generation of garnet (Grt 2) is associated with K-feldspar and cordierite intergrowths (Ksp+Crd) and fine-grained, dendritic

orthopyroxene (Opx) (Figure 2f). The K-feldspar and cordierite intergrowths are disseminated throughout the rock, with and without garnet 2 (Figure 2g), and are interpreted to have formed via the breakdown of osumilite. A third generation of garnet (Grt 3) forms textural overgrowths on quartz. Three texturally distinct zircon morphologies are revealed through CL imaging, with both CL high (Ch)- and low (Cl)-response cores observed with a number of grains displaying high-CL response rims (Rh) (Figure 3c).

Sample 171279-9 comprises coarse-grained garnet (Grt 1), orthopyroxene, mesoperthite (Fsp) and quartz (Figure 2h). The coarse-grained quartz (Qz(Rt)) contains abundant rutile needles whose orientations appear to be crystallographically controlled (Figure 2i). Coarse-grained garnet is mantled by a second generation of fine-grained garnet (Grt 2) (Figure 2h). Zircon grains display a variety of CL textures with both high (Ch)- and low (Cl)-response cores observed (Figure 3d); high (Rh)- and low (Rl)-response rims and a number of sector-zoned, high-response grains (Sh) were also present.
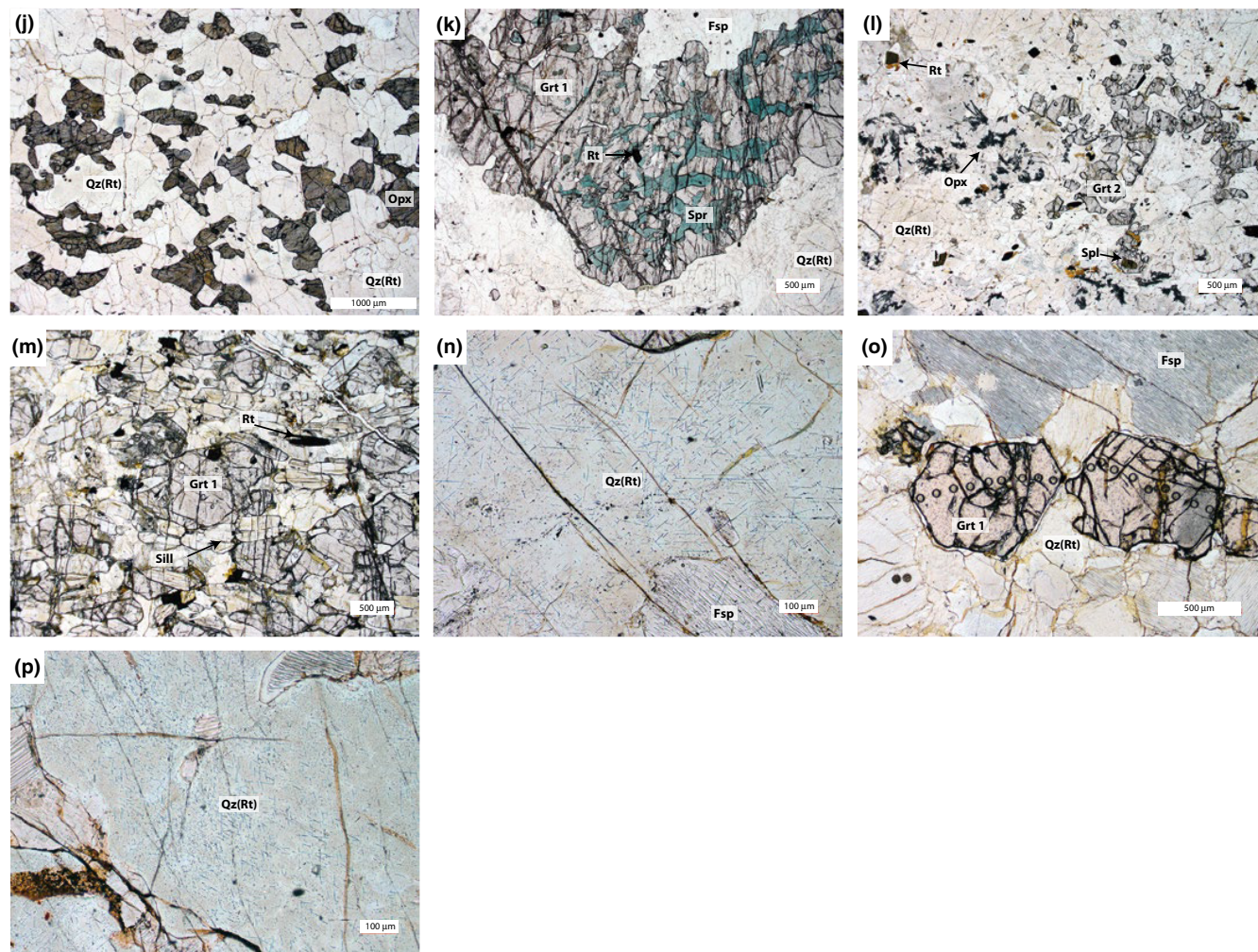
FIGURE 2 Continued

Sample 171279-10 (previously reported as 171279-1 in Taylor et al., 2017) contains a relatively simple mineralogy of orthopyroxene (Opx), quartz (Qz(Rt)) with rutile exsolution lamellae and K-feldspar (Figure 2j). Zircon grains display both high (Ch) and low (Cl) CL response cores, some of which have high-Cl response, recrystallized rims (Rh) (Figure 3e).

4.3 | Mount Hardy

Sample 91279-13 is a spectacular rock that contains coarse-grained garnet (Grt 1) intergrown with blue sapphirine (Spr) in a matrix of rutile-bearing quartz (Qz(Rt)) and mesoperthite (Fsp); both the matrix and garnet 1 contain rutile grains (Figure 2k,l). A second generation of garnet (Grt 2) is associated with intergrowths of K-feldspar, cordierite and fine-grained, dendritic orthopyroxene (Opx); garnet 2 contains inclusions of spinel (Spl). These intergrowths are inferred to result from the breakdown of osumilite that formed part of the peak coarse-grained assemblage. Zircon grains have a uniformly low-CL

response, with some grains preserving igneous shapes and barely discernable oscillatory zoning (Cl), while others have faint sector zoning (Sl) (Figure 3f).

4.4 | Mount Harvey

Sample 3180-2 is a garnet (Grt 1), sillimanite (Sill), quartz (Qz(Rt)), mesoperthite (Fsp) gneiss containing accessory rutile (Rt) (Figure 2m,n). Quartz contains crystallographically controlled rutile exsolution lamellae (Figure 2n). Zircon grains are dominantly sector-zoned with low-CL response (Sl). There is a subordinate population of sector-zoned grains with a moderate- to high-CL response (Sh). Rare grains of zircon that are interpreted to have inherited cores were observed; they exhibit both high (Ch)- and low (Cl)-CL responses (Figure 3g).

4.5 | Mount Denham

Sample 3180/7 comprises simply garnet (Grt 1), quartz (Qz(Rt)) and mesoperthite (Fsp) (Figure 2o). Quartz contains
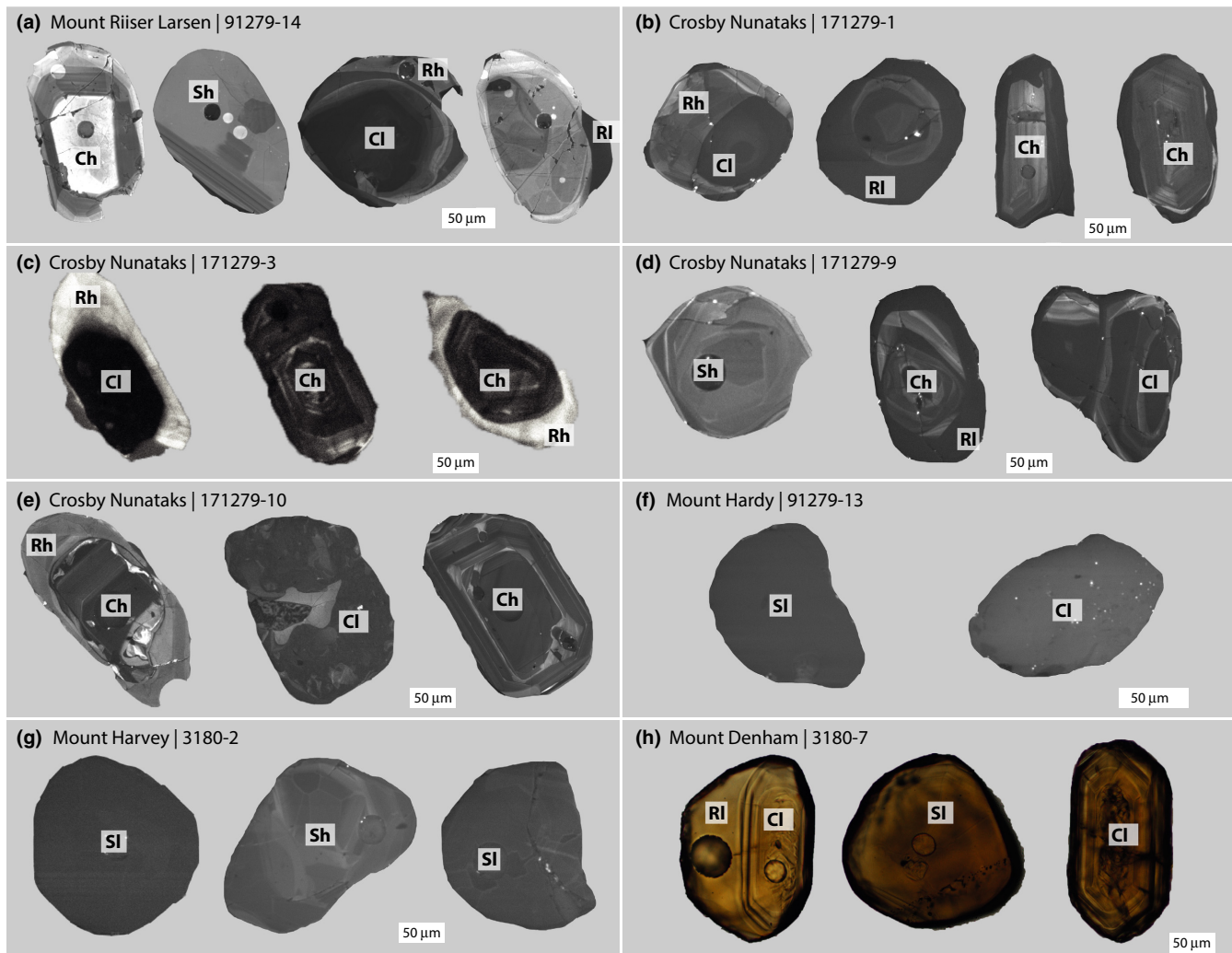
FIGURE 3 (a–g) Cathodoluminescence (CL) images of representative zircon grains highlighting the variations in internal structures targeted for geochronological investigation. (h) Transmitted light images of zircon from Mount Denham, CL imaging provided was uniformly low response, whereas transmitted light imaging provided textural information for targeting. For the locations of all analyses, the reader is referred to Figure S2. Ch—core high-CL response; Cl—core low-CL response; Rh—rim high-CL response; Rl—rim low-CL response; Sh—sector-zoned high-CL response; Sl—sector-zoned low-CL response

exsolution lamellae of rutile (Figure 2p). Zircon grains have a uniformly low-CL response. However, when viewed under transmitted light, oscillatory-zoned cores (Cl) with and without rims (Rl), and entirely new grains display sector zoning (Sl) (Figure 3h).

5 | RESULTS

The U–Pb, trace element and Ti-in-zircon thermometry analyses of zircon and garnet from the Tula Mountains are summarized in Table 1 and Figures 4–6. Here we summarize the key features for each sample; the reader is referred to the accompanying supplementary data sets for the full analytical results. All ages are reported at the 2σ level and the corresponding number of analyses and MSWD can be found in Table 1. The full set of results are available in Supporting Information Tables S1 and S2; Concordia plots for the individual zircon textures and spot locations for all analysed zircon grains are provided in Supporting Information Figures S1 and S2.

Sample 91279-14: Zircon U–Pb ages from this sample returned five concordant populations with zircon rims returning the oldest concordant ages ($2,470 \pm 16$ Ma and $2,460 \pm 11$ Ma), sector-zoned zircon ages returned slightly younger concordant ages ($2,455 \pm 11$ Ma and $2,443 \pm 14$ Ma). The youngest concordant age is $2,439 \pm 14$ Ma from the high-CL response cores (these cores did not have analysable rims), and low-CL response cores returned a range of concordant dates from 2,505 to 2,434 Ma. All of the concordant populations of zircon display positive HREE slopes with Yb_n/Gd_n generally <10;
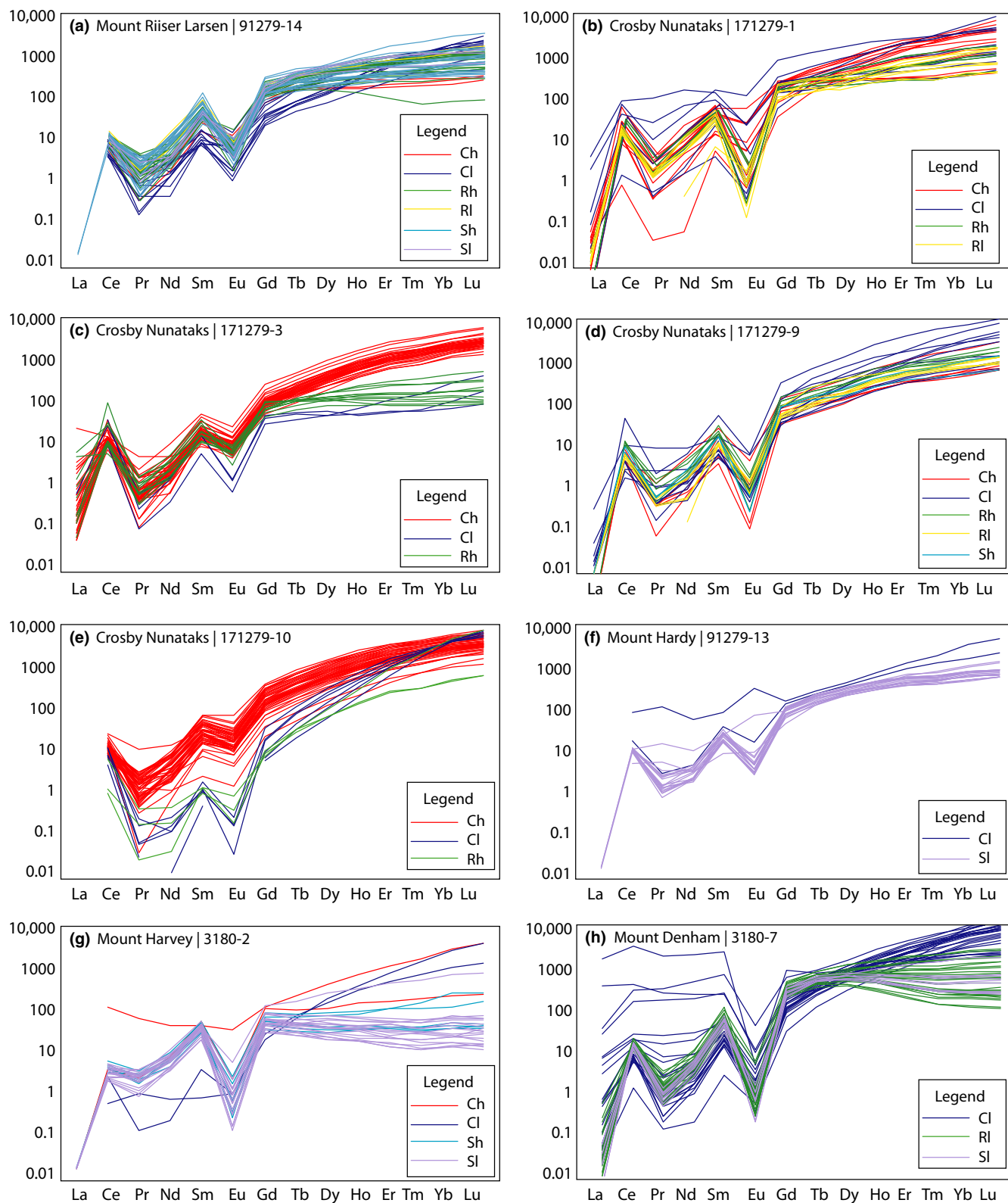
FIGURE 4 (a–h) Chondrite normalized REE plots for zircon grains analysed in this study; line colours represent different zircon cathodoluminescence (CL) textures. Ch—core high-CL response; Cl—core low-CL response; Rh—rim high-CL response; Rl—rim low-CL response; Sh—sector-zoned high-CL response; Sl—sector-zoned low-CL response
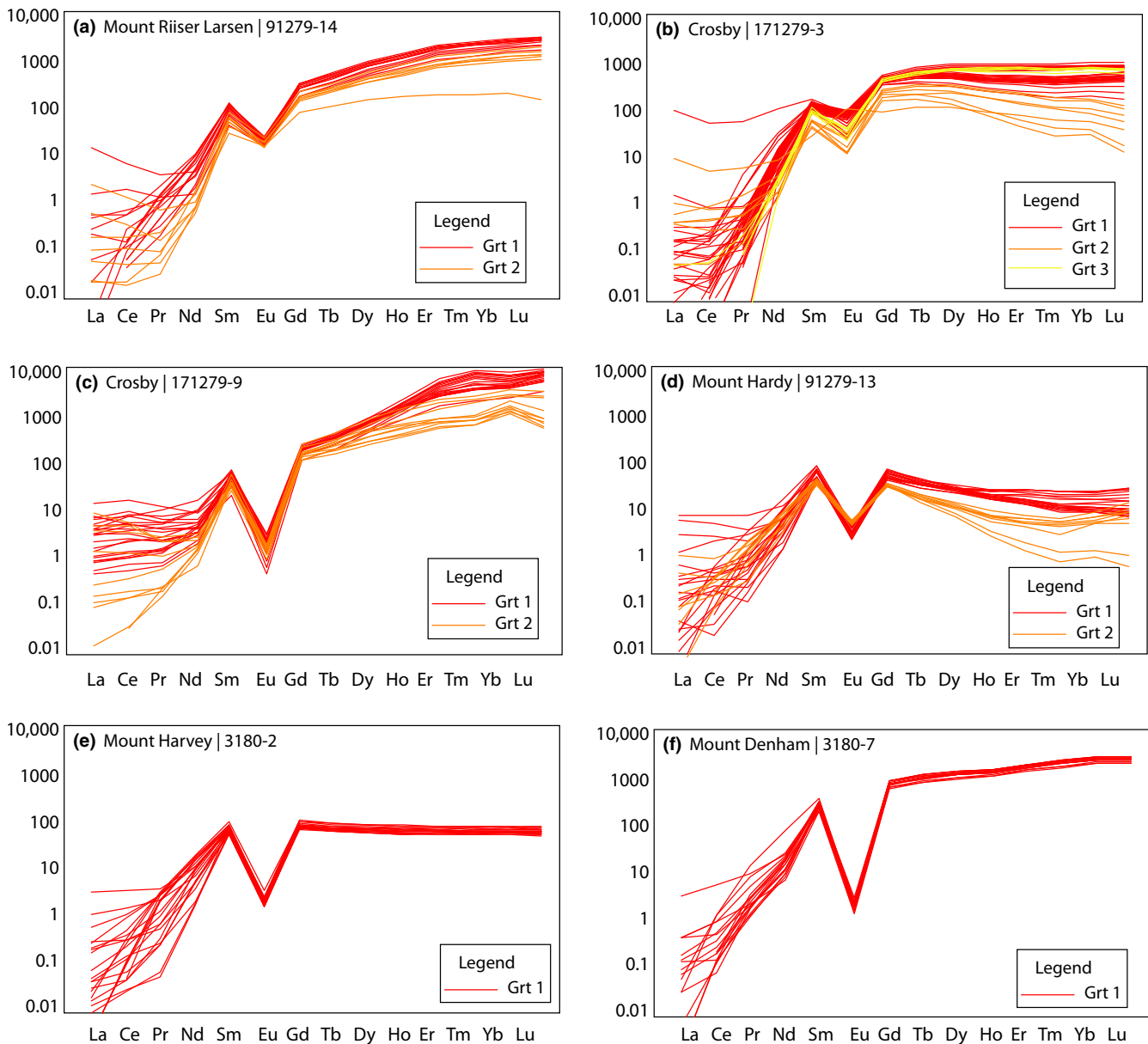
the low-CL response cores show a wider spread of Yb_n/Gd_n from <10 to 44 (Figure 4a). The Th/U ratios of zircon grains are typically greater than the suggested metamorphic value of 0.1, but consistent with the Th/U ratios from other UHT terranes as documented in Rubatto (2017), Shaffer et al. (2017) and Yakymchuk, Kirkland, and Clark (2018).

FIGURE 5 (a–h) Box-and-whisker plots for Ti-in-zircon temperatures for each zircon textures. For the summary of results, the reader is referred to Table 1. Ch—core high-CL response; Cl—core low-CL response; Rh—rim high-CL response; Rl—rim low-CL response; Sh—sector-zoned high-CL response; Sl—sector-zoned low-CL response

FIGURE 6 (a–f) Chondrite normalized REE plots for garnet grains analysed in this study; line colours represent different garnet generations

Ti-in-zircon thermometry yielded temperatures >900°C for four of the six concordant populations; however, the youngest sector-zoned population and the high-CL response cores have calculated temperatures of 847 and 894°C (Figure 5a). Garnet grains in this sample also have positive HREE slopes Yb_n/Gd_n <10, with garnet 2 having slightly lower Yb_n/Gd_n and a less pronounced Eu anomaly than garnet 1 (Figure 6a).

Sample 171279-1: Two concordia ages (2,475 ± 15 Ma and 2,490 ± 10 Ma) were obtained from high- and low-CL response zircon rims; the zircon cores yielded a spread of dates with an upper limit of *c*. 2,840 Ma spreading down to a cluster of dates at *c*. 2,480 Ma. All zircon grains display positive HREE slopes, with the rims showing less

spread (Yb_n/Gd_n: 1–11) than the cores (Yb_n/Gd_n: 1–87; Figure 4b). The Th/U ratios range from 0.02 to 2.9 and show no correlation with age or CL texture. Ti-in-zircon thermometry returns a relatively restricted range of 858–897°C, with the rims falling at the colder end of the range (Figure 5b).

Sample 171279-3: The bulk of zircon in this sample has high-CL response cores and displays a spread in U–Pb ages from 2,849 to 2,457 Ma, with most clustering around *c*. 2,840 Ma. Two concordia ages were calculated for low-CL response cores (2,457 ± 33 Ma) and high-CL response rims (2,454 ± 9 Ma). High-Cl response cores show distinctly steeper HREE slopes (Yb_n/Gd_n of up to 21) than the low-CL response cores (1.5–4) and high-CL response

rims (1.4–5.4) (Figure 4c). Ti-in-zircon thermometry for both high-CL response cores and rims returned temperatures of 904°C, with the low-CL response rims having a lower calculated temperature of 871°C (Figure 5c). Garnet 1 displays slightly negative HREE slopes (Yb_n/Gd_n: 0.18–0.63), whereas garnet 2 and 3 have flat to positive HREE slopes; all display a similar range of negative Eu anomalies (Figure 6b).

Sample 171279-9: Four concordia ages from 2,502 ± 24 Ma to 2,470 ± 13 Ma were obtained from the various CL textures; low-response CL cores yielded a spread of concordant dates from 2,691 to 2,427 Ma, but no concordia age. All zircon grains display positive HREE slopes with Yb_n/Gd_n values from 5 to 75 (Figure 4d). Ti-in-zircon thermometry yielded temperatures >900°C for all crystals (Figure 5d). The Th/U ratios are tightly clustered between 0.02 and 0.7. All garnet grains have positive HREE slopes, with garnet 1 displaying steeper positive slopes than garnet 2 (Figure 6c).

Sample 171279-10: Zircon grains from this sample returned only one concordia age for the high-CL response rims (2,483 ± 16 Ma); the high-CL response cores yielded a spread of dates from 2,858 to 2,486 Ma, with the bulk of ages clustering at *c*. 2,850 Ma, while the low-CL response cores cluster between 2,600 and 2,500 Ma. All zircon groups display steeply positive (Yb_n/Gd_n: >10) HREE patterns (Figure 4e) and Th/U ratios >0.1. Ti-in-zircon thermometry yields temperatures of >940°C for both types of zircon cores and 856°C for the high-CL response zircon rims (Figure 5e).

Sample 91279-13: This sample is dominated by a single concordant population of low-CL response sector-zoned grains that return a concordia age of 2,492 ± 7 Ma; two other analyses from low-CL response cores return dates of 2,665 and 2,352 Ma. All sector-zoned zircon has positive HREE slopes (Figure 4f), Th/U ratios between 0.10 and 0.38, and yields a Ti-in-zircon temperature of 914°C (Figure 5f). The two generations of garnet in this sample display weak negative HREE slopes with Yb_n/Gd_n values between 0.04 and 0.52 (Figure 6d).

Sample 3180-2: Two concordant populations of sector-zoned zircon grains are observed in this sample; high-CL response grains return an age of 2,454 ± 11 Ma and low-CL response grains have an age of 2,461 ± 7 Ma. Both populations are dominated by slightly negative to flat HREE patterns (Figure 4g), Th/U ratios of >0.1 to 1.61 and Ti-in-zircon temperatures of ~900°C (Figure 5g). Garnet in this sample has tightly grouped weakly negative HREE slopes with Yb_n/Gd_n of between 0.73 and 0.84 (Figure 6e).

Sample 3180-7: Low-CL response rims and sector-zoned zircon grains in this sample yield concordia ages of 2,471 ± 7 Ma and 2,474 ± 5 Ma respectively. Low-CL response cores display a spread of concordant dates that

ranges from 2,609 to 2,431 Ma. The zircon rims and sector-zoned grains display a wide range of weakly negative to slightly positive HREE patterns (Yb_n/Gd_n of 0.37–5.5 and 0.56–7.9 respectively), while the cores have strongly positive slopes with Yb_n/Gd_n of 5.8–95 (Figure 4h). The Th/U ratios of the rims and sector-zoned grains (up to 0.17) are slightly lower than those obtained from the zircon cores (up to 0.50). Ti-in-zircon thermometry from all grains returns relatively consistent temperatures between 828 and 843°C. Garnet in this sample shows a tightly grouped weakly positive HREE slopes (Figure 6f).

6 | DISCUSSION

6.1 | An assessment of zircon–garnet equilibrium

The control exerted on the REE uptake of zircon by coexisting garnet has been well documented both empirically (Hermann & Rubatto, 2003; Rubatto, 2002; Rubatto & Hermann, 2003; Schaltegger et al., 1999; Whitehouse & Platt, 2003) and experimentally (Rubatto & Hermann, 2007; Taylor, Harley, et al., 2015). The zircon–garnet partitioning relationship is often assessed through interpretation of HREE patterns of zircon or the construction of D_{REE}(zircon–garnet) plots that are then visually compared to the appropriate experimental data sets of Rubatto and Hermann (2007) or Taylor, Harley, et al. (2015). These methods have been used to great effect in a number of studies where the range of zircon and garnet chemistry and morphologies are relatively simple (Clark et al., 2009, 2015; Gauthiez-Putallaz, Rubatto, & Hermann, 2016; Hermann & Rubatto, 2003; Kotková & Harley, 2010; Kotková, Whitehouse, Schaltegger, & D'Abzac, 2016; Kylander-Clark & Hacker, 2014; MacDonald et al., 2015; Štípská et al., 2016). The utility of these techniques in visualizing equilibrium relationships in terranes that have experienced multiple episodes or protracted durations of metamorphism becomes increasingly complex as zircon undergoes varying degrees of recrystallization, re-equilibration and neocrystallization. In these cases, care must be taken to identify zircon and garnet chemical compositions that reflect the timing of growth and breakdown; this is difficult if average REE patterns are used for each zircon population (e.g. Kelly & Harley, 2005).

In an effort to handle larger and more complicated data sets, Taylor et al. (2017) proposed plotting log (D_{Yb}/D_{Gd}) versus log(D_{Yb}) for individual zircon grains against selected garnet compositions. These parameters are the most sensitive to environmental conditions and therefore key for identifying partitioning of REE between zircon and garnet during metamorphic events. Here we employ these plots to assess the timing of the different textural types of zircon relative to the
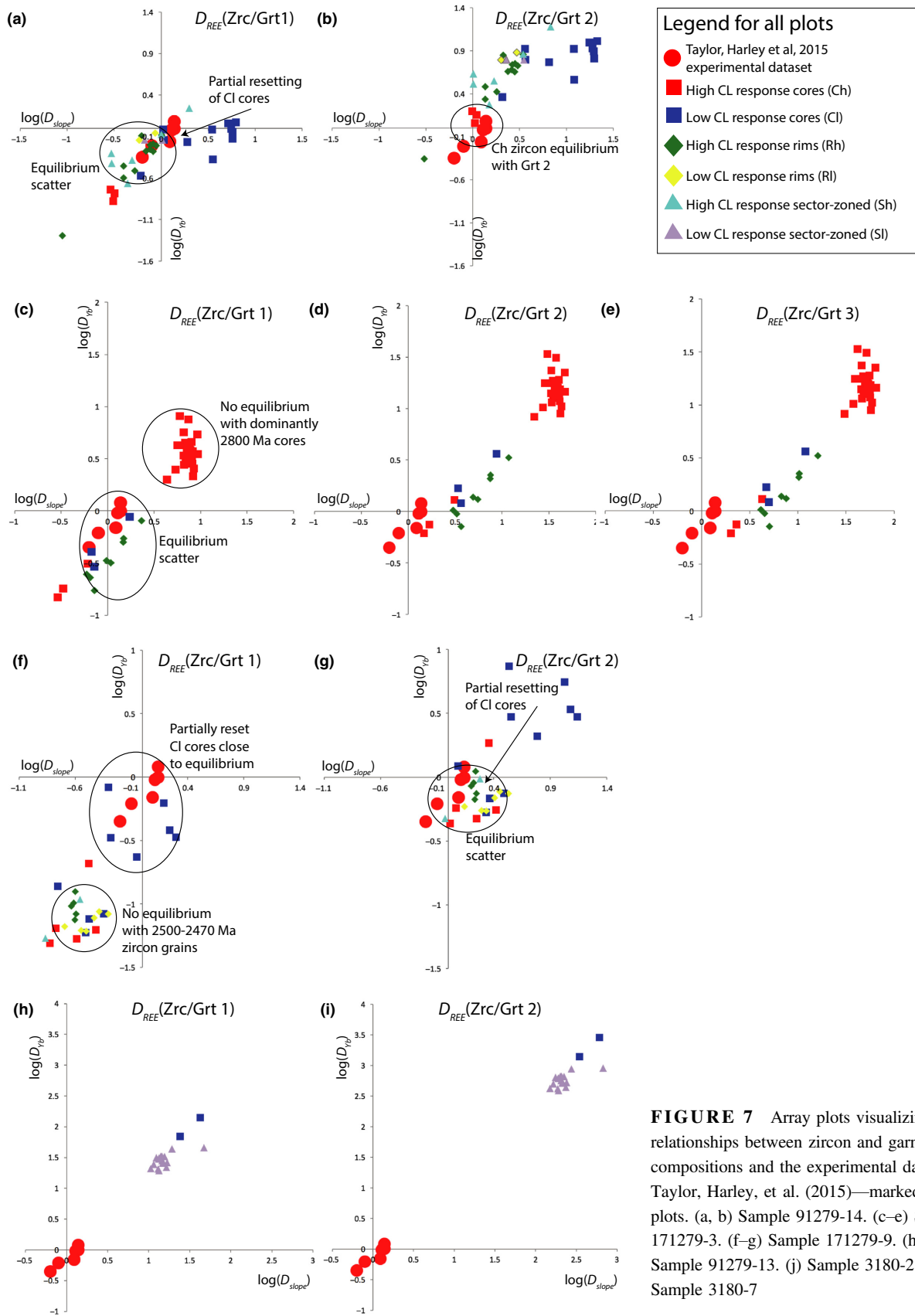
FIGURE 7 Array plots visualizing the relationships between zircon and garnet REE compositions and the experimental data set of Taylor, Harley, et al. (2015)—marked as XP in plots. (a, b) Sample 91279-14. (c–e) Sample 171279-3. (f–g) Sample 171279-9. (h–i) Sample 91279-13. (j) Sample 3180-2. (k) Sample 3180-7
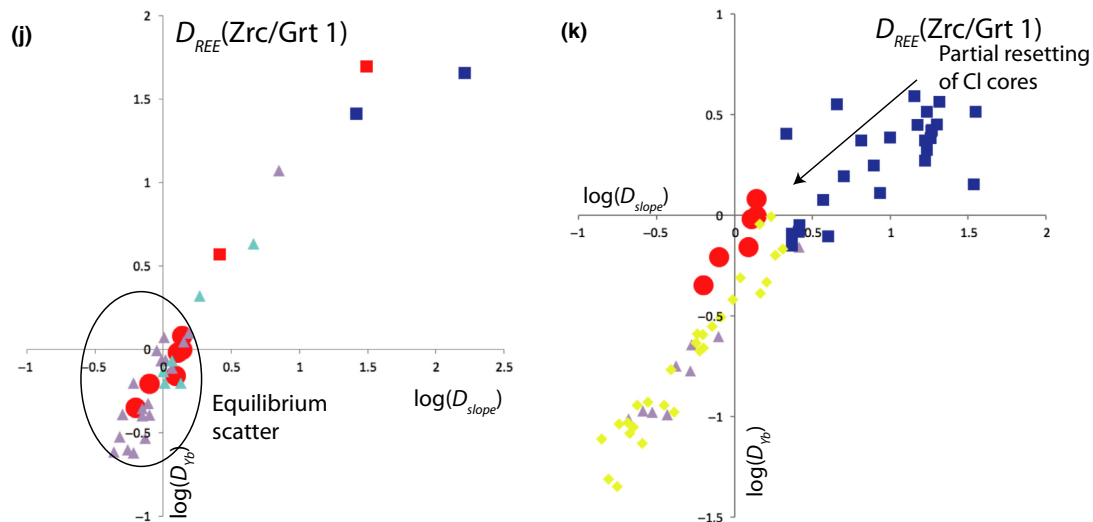
FIGURE 7 Continued

garnet generations identified earlier. We plot them relative to the experimental data set of Taylor, Harley, et al. (2015) because the *P–T* conditions of those experiments are close to those experienced by the rocks of the Napier Complex; the experiments of Rubatto and Hermann (2007) may be more suitable for higher pressure rocks.

At Mount Riiser Larsen (sample 91279-14), zircon rims and sector-zoned zircon grains plot close to the experimental data of Taylor, Harley, et al. (2015) when compared to garnet 1 but not garnet 2 (Figure 7a), suggestive of equilibrium with coarse-grained garnet 1. Low-response cores show no equilibrium relationship with either garnet 1 or 2. They do however track towards the experimental data when plotted against garnet 1, potentially indicating progressive, but incomplete, recrystallization of these grains controlled by garnet 1 (Figure 7a). The high-CL response cores plot close to the experimental data when compared to garnet 2; this may indicate zircon remained in communication with the texturally late garnet 2, consistent with it returning the youngest age (Figure 7a,b; Table 1). There are two samples from Crosby Nunataks containing zircon and garnet. In sample 171279-3, rims and low-CL response cores show an equilibrium relationship with the coarse-grained, peak garnet 1 (Figure 7c). The high-CL response cores that have a dominant age cluster of *c.* 2,850 Ma show no equilibrium relationship with either garnet 1, 2 or 3, consistent with their steep HREE slopes (Figures 4c and 7a–c). Garnet generations 2 and 3 appear not be in equilibrium with any zircon despite having characteristic flat HREE patterns like the *c.* 2,450 Ma zircon populations in this sample (Figures 4c, 5b and 7c–e). This highlights the danger of assessing zircon–garnet relationships only by observing the shape of the HREE patterns in isolation. Zircon and garnet from sample 171279-9 both display positively sloping HREE patterns (Figures 4d and 5c). Concordant zircon

populations with ages ranging between 2,500 and 2,470 Ma are not in equilibrium with the coarse-grained garnet 1 (Figure 7f) but are close to equilibrium with the finer grained garnet 2 (Figures 2h and 7g). Low-CL response zircon cores that show variable resetting of the U–Pb system scatter around the expected equilibrium range with garnet 1 (Figure 7f) but also show a tendency to be drawn towards equilibrium with garnet 2 (Figure 7g). We interpret garnet 1 in this rock to have formed during an earlier magmatic/metamorphic event at *c.* 2,850 Ma, and garnet 2 to have formed during the metamorphic event at *c.* 2,500 Ma. Interestingly, when the HREE patterns for zircon (Figure 4c) from this sample are viewed in isolation, the positive slopes for the *c.* 2,500 Ma zircon populations would not be interpreted to have grown in communication with garnet. Zircon grains from Mount Hardy (sample 91279-13) are significantly enriched in HREE when compared to the two generations of garnet (Figures 4f and 5d), resulting in them plotting quite a distance from the experimental data set (Figure 7h,i). This suggests that zircon was not in communication with garnet during the formation of the peak assemblage (garnet 1+sapphirine+osumilite) or during the breakdown of osumilite to form garnet 2. At Mount Harvey, a garnet 1+sillimanite+rutile gneiss (sample 3180-2) displays classic flat HREE patterns for both 2,450 Ma zircon and garnet (Figures 4g and 5e). When plotted against the experimental data set of Taylor, Harley, et al. (2015), the 2,450 Ma zircon–garnet pairs directly overlap the experimental data (Figure 7j). Sample 3180-7 contains a few zircon grains that display some degree of equilibrium with garnet (Figure 7k); however, both of the 2,470 Ma populations of zircon have an order of magnitude variation in their normalized HREE abundances (Figure 4h). The textural characteristics of this rock (euhedral garnet in a dominantly quartz and feldspar matrix) suggest

that it is a leucosome and the garnet may be entrained peritectic grains. Low-CL response cores show a trend towards the experimental data set (and equilibrium with garnet), potentially representing partial resetting in the presence of melt, whereas the rims and neocrystallized zircon grains formed in an environment where garnet did not exert a significant control over the zircon chemistry—most likely during the final crystallization of the leucosome (Figure 7k).

In summary, the bulk of the 2,500–2,440 Ma zircon grew or recrystallized in equilibrium with garnet that forms part of the peak metamorphic assemblages from across the Tula Mountains. In contrast, the texturally late garnet in most samples (apart from sample 171279-9) is not in equilibrium with zircon and most likely grew after zircon during the final stages of melt crystallization (e.g. during osumilite breakdown), although some garnet may have exerted a limited control on recrystallizing zircon cores. For sample 171279-9, we suggest that the coarse-grained assemblage of garnet and orthopyroxene formed during an earlier magmatic/metamorphic event, although we are unable to definitively state whether this assemblage is magmatic or metamorphic.

6.2 | High-T history of the Napier Complex

There are two main questions that remain unresolved with regard to the high-T evolution of the Napier Complex. The first is the timing and conditions of the regional, pre-2,500 Ma magmatic/metamorphic event tentatively identified by Kelly and Harley (2005). The second is how long the Napier Complex resided at high to UHT metamorphic conditions. The zircon–garnet relationships described in the previous section combined with the newly acquired Ti-in-zircon thermometry from these rocks and observations from previous studies go some way in resolving these two issues.

6.2.1 | Timing and conditions of the $c.$ 2,850 Ma event

Kelly and Harley (2005) identified growth of new zircon between 2,850 and 2,840 Ma from Proclamation Island and Dallwitz Nunatak and Pb-loss discordia trending towards 2,850 Ma. They suggested that this was a low-P, high-T event due to positively sloping HREE patterns of zircon. They also speculated that this event was not UHT, although the evidence behind this speculation is unclear. A number of samples from the Crosby Nunataks preserve zircon with ages of $c.$ 2,850 Ma, and most display Pb-loss trends anchored at $c.$ 2,500 Ma. All of the $c.$ 2,850 ages were obtained from zircon cores exhibiting oscillatory zoning—a feature most commonly associated with igneous zircon, rather than zircon crystallizing from anatectic melt (Taylor, Kirkland, & Clark, 2016). These zircon populations all display positive HREE slopes consistent with the

observation of Kelly and Harley (2005). However, sample 171279-9 contains garnet that also displays a steep HREE pattern, and the associated array plot suggests that some zircon cores retain an equilibrium relationship with garnet. As stated previously, we interpret the garnet 1 in this rock to have formed during the 2,850 Ma event although we cannot unequivocally assess whether it is magmatic or metamorphic. Our preferred interpretation is that garnet is peritectic and was entrained during the ascent of the magmatic protolith to the orthogneiss.

The temperature of this event has largely been obscured by the overprinting 2,500 Ma event. In this study, a number of samples preserve concordant or near concordant U–Pb ages and have Ti-in-zircon temperatures that range from 895 to 943°C (Table 1; Figure 5b,c,e). These temperatures, in combination with the consistently positive HREE slopes (i.e. zircon growth in the absence of the high-P mineral garnet) and grain oscillatory zoning, are consistent with zircon growth during the crystallization of high-T magma. Our data reinforce the previous interpretation that this event was low pressure/high temperature. We further suggest that metamorphism at $c.$ 2,850 Ma was driven by the emplacement of large volumes of high-temperature charnockitic/felsic magmas and that this event should also be considered a regional UHT event.

6.2.2 | Residence time at UHT

The onset of UHT metamorphism in the Napier Complex has been inferred by Harley (2016) and Harley et al. (2001) to have begun at 2,585 Ma based on concordant zircon from McIntyre Island that demonstrate REE equilibrium with garnet from UHT leucosomes. Follow-up Ti-in-zircon thermometry on these grains undertaken by Harley (2016) yielded temperatures of ~915°C confirming that the grains either grew or were recrystallized at UHT. Carson, Ague, and Coath (2002) reported zircon ages of 2,546 Ma from Tonagh Island that they interpreted to have grown at UHT; they also reported the emplacement of a 2,620 Ma orthogneiss, putting an upper limit on the age of the UHT event. Horie et al. (2012) reported a detrital zircon age of 2,580 Ma from Mount Cronus that they proposed provides a maximum age constraint on UHT metamorphism in the Napier Complex. This age overlaps with the Harley et al. (2001) age constraint on zircon growth in leucosomes and requires that the onset of crustal temperatures >900°C and sedimentation were coincident, a scenario that is difficult to envisage. Given that the age constraints on both sedimentation and metamorphism are purported to be from concordant grains, this overlap can be explained by two contrasting scenarios: (a) the onset of metamorphism varied across the terrane and the ages reflect sedimentation coincident with mid-crustal UHT metamorphism or (b) processes

that operate at the grain-scale affected the U–Pb ages recorded by individual zircon grains.

Scenario 2 is our preferred option as it is difficult to envisage a tectonic scenario whereby rocks that began experiencing UHT conditions at 2,585 Ma were subsequently juxtaposed against sediments that were being deposited concurrently and then all followed the same cooling path simultaneously growing large significant new zircon between 2,500 and 2,450 Ma. Kusiak et al. (2013) and Piazolo et al. (2016) have demonstrated in rocks from the Napier Complex that Pb is mobile within zircon grains and that this mobility leads to both older and younger ages from disturbed grains that are within error of concordia. The method employed by both Harley et al. (2001) and Horie et al. (2012), namely secondary ionization mass spectrometry (SIMS), is particularly susceptible to this type of disturbance due to the small analytical volume and the size of the Pb-enriched areas. This process is more likely to impact inherited grains because they have sufficient ingrown radiogenic Pb, and experience the full duration of the high-T event as opposed to neocrystallized metamorphic grains such as those reported by Harley (2016) and Harley et al. (2001). In addition, the analytical resolution of the SIMS technique, and the slope of concordia between c. 2,700 and 2,500 Ma act to mask high-T Pb loss. We therefore interpret (a) the depositional ages of Horie et al. (2012)—in the absence of evidence against Pb mobility either through gain or loss—as based on grains that have lost Pb; and (b) the Harley et al. (2001) and Harley (2016) ages of c. 2,580 Ma as representing the onset of metamorphism in the Napier Complex. The c. 2,620 Ma age of the orthogneiss dated by Carson, Ague, and Coath (2002) is taken as the maximum age constraint of UHT metamorphism in the Napier Complex. Although, it is possible that the zircon in this sample experienced the same Pb-modifiying processes as outlined above. However, we consider it less likely to have affected the final age to any significant degree because the age is based on analysis of multiple grains and is defined by a concordia-intercept age that is less susceptible than a weighted average based on $^{207}Pb/^{206}Pb$ ages (e.g. Kusiak et al., 2013).

The bulk of metamorphic zircon growth in the Napier Complex occurred from 2,500 to 2,450 Ma and has been interpreted to reflect post-peak crystallization of zircon below UHT at or near the solidus (e.g. Harley, 2016; Kelly & Harley, 2005). This is consistent with the observation by Tomkins et al. (2007) that metamorphic zircon overgrowths in granulites are unlikely to be the product of peak metamorphism and must relate to the time of retrograde cooling, and by Korhonen, Clark, Brown, Bhattacharya, and Taylor (2013) who argued that U–Pb ages from zircon overgrowths from UHT rocks in the Eastern Ghats Province record cooling to the solidus. While we

acknowledge that at the durations and the conditions proposed in this study Pb may be mobile in zircon, the application of concordia ages argues definitively against diffusional resetting of the Pb system in the zircon populations used in interpreting the duration of events in this study. Where there is evidence of Pb loss and no concordia age was calculated, the ages are treated with appropriate caution. While there is always the potential for diffusion and modification, the statistically robust age check afforded through the application of the two systems (U–Pb and Pb–Pb) to determine ages of zircon growth provides a check on the potential role of Pb loss.

The present study demonstrates 900°C Ti-in-zircon minimum temperatures for the bulk of zircon in the range 2,500–2,450 Ma (Table 1; Figure 5). Some samples have crystallization temperatures below 900°C, but these rocks do not contain rutile and therefore yield minimum estimates of temperature (Ferry & Watson, 2007). Using phase equilibria modelling, Yakymchuk, Clark, and White (2017) demonstrated that the activity of TiO_2 in rocks on the retrograde path tends to be less than 1 even if the rock retains rutile, such that the zircon temperature estimates from this study provide definitive evidence that UHT prevailed in the crust and that zircon grew in equilibrium with the peak assemblage until at least 2,450 Ma (Figure 5; Table 1). The argument of Kelly and Harley (2005) that most zircon grows at less than 900°C as it crystallizes at the solidus (which they infer to be between 900–800°C) fails to take in to account that zircon saturation and growth occur above the solidus (e.g. Kelsey, Clark, & Hand, 2008). In addition, highly residual granulites, such as those observed throughout the Napier Complex, likely have elevated solidi, a feature observed in other UHT terranes (e.g. Korhonen et al., 2013). The data from this study, when combined with the age constraints for the onset of UHT, suggest that the duration of the high-T event in the Napier Complex was on the order of 135 Ma, spanning 2,585–2,450 Ma.

6.3 | Metamorphic drivers

Identification of regional UHT metamorphism that persisted for >100 Ma is becoming more common, with examples including the Eastern Ghats Province (Kelsey et al., 2017; Korhonen et al., 2013), the East African Orogen (Clark et al., 2015; Fitzsimons, 2016; Harley, 2016; Horton et al., 2016) and the Musgrave Orogen (Walsh et al., 2015). There are relatively few large-scale, long-lived heat sources available to sustain UHT in the crust for >100 Ma. Potential heat sources include elevated mantle temperatures, long-lived high-T magmatism and radiogenic self-heating. Other heat sources such as shear heating may contribute in the early stages of metamorphism but once the rocks begin to melt this mechanism becomes ineffective (Clark,

Fitzsimons, Healy, & Harley, 2011; Nabelek, Whttington, & Hofmeister, 2010).

In the specific case of the Napier Complex, the geochronological and petrological data point towards a scenario in which UHT was achieved at a maximum of *c.* 40 Ma after burial commenced, and the UHT then lasted for another 135 Ma (Carson, Ague, & Coath, 2002; Harley, 2016). Mantle temperatures at *c.* 2,500 Ma would have been on the order of 150–250°C above the present day—certainly a contributor to the overall thermal regime, but alone insufficient to raise and sustain the temperatures observed in the Napier Complex (Brown & Johnson, 2018). There is also a distinct absence of any evidence of large volumes of synmetamorphic intrusions of appropriate temperatures over this time interval that could have driven and sustained the observed metamorphic conditions (Harley, 2016; Sheraton, Tingey, et al., 1987). While it is possible that the earlier stages of UHT metamorphism recognized by Harley et al. (2001) reflect one or more short pulses of localized heating (Pownall, Hall, Armstrong, & Forster, 2014) and do not reflect UHT conditions being achieved across the terrane at this time, the absence of any magmatism that can be directly linked to this early stage argues against this scenario. However, it needs to be acknowledged that such small pulses of heating at the start of an orogeny could be important in achieving the regional-scale peak conditions observed (Pownall et al., 2014; Viete & Lister, 2017). It would be very difficult to recognize these localized, short-duration heating events in the current rock record as they would be significantly modified and obscured by regional-scale UHT event that follows.

In a number of long-lived, regional UHT terranes, the burial of radioactive heat-producing elements (HPE) has been interpreted as the key to attaining high temperatures for the prolonged durations observed (Clark et al., 2015; Horton et al., 2016; Korhonen et al., 2013). Clark et al. (2011) demonstrated that UHT can be achieved in the crust through radiogenic self-heating in the absence of large volumes of magmatism. However, they pointed out that the latent heat of fusion has a significant impact on the temperature rise in the crust, with UHT being reached only after *c.* 60 Ma of burial of crust with radioactive heat production of 3.5–4 $\mu W/m^3$. While this looks to be longer than the time available in the Napier Complex, there are some factors that could contribute to reducing the required time to heat and maintain UHT. First, the regional UHT event at *c.* 2,850 Ma would have produced a less-fertile terrane with a reduced capability of thermally buffering temperature, i.e. the terrane was preconditioned. Second, the average levels of HPE in Archean crustal rocks were ~2 times the present day (Black, Sheraton, et al., 1986). In order to maintain the temperatures for long durations, the HPEs must be retained in the mid- to lower crust rather than be removed during partial melting. Bea

(2012) and Alessio et al. (2018) demonstrated that HPEs are not efficiently removed from the lower crust by partial melting, contradicting the widely held view that melt loss removes these elements from the mid to lower crust (e.g. Jaupart, Mareschal, & Iarotsky, 2016). However, if heating progresses long enough, all the repositories of U and Th (monazite and zircon) may dissolve in to melt (Kelsey et al., 2008). In the Napier Complex, there is a distinct lack of monazite in the residual rocks, suggesting that melt extraction has removed the constituents that form monazite (LREE, P and Th); the lack of monazite growth during cooling is reflected in the elevated (>0.1) Th/U ratios of the zircon analysed in this study. High Th/U ratios are a common feature in many UHT rocks (Rubatto, 2017; Yakymchuk et al., 2018) indicating that there is a threshold in the stability of monazite at extreme temperatures. Once this temperature is exceeded, there will be a significant reduction in the HPE content of the lower crust and the rocks will begin to cool when the heat source is removed.

The timing of UHT metamorphism in the Napier Complex is also significant as it occurs at the same time as the continents were aggregating into supercratons. While it is impossible to constrain the exact palaeogeographic position of the Napier Complex, it is not unreasonable to assume that it was involved in supercraton amalgamation. Collins (2002) and Brown (2007) have postulated that tectonic settings prior to the formation of supercontinents will be dominated by back-arc basins, regions with enhanced heat flow (e.g. Hyndman & Currie, 2011; Hyndman, Currie, & Mazzotti, 2005). This type of tectonic setting will thermally prime the crust and lead to the generation of high thermal gradients. As the supercontinent coalesces, collisional orogens effectively bury large volumes of crustal material (enriched in HPEs) under a slowly eroding orogenic plateau (Hacker, Ritzwoller, & Xie, 2014; Hacker et al., 2000). Harley (2016) proposed the Napier Complex formed the root of a large and hot collisional orogen. We broadly agree with this characterization of the tectonic setting of the Napier Complex, with the refinements that the Napier Complex had been preconditioned by an earlier *c.* 2,850 Ma UHT event, experienced enhanced mantle heat flow through both elevated mantle temperatures and crustal thinning (at the onset of orogenesis) and that the HPEs (the primary heat source) were removed late in the history of the orogeny (after temperatures exceeded UHT). All of these factors contributed to the thermally extreme, regional metamorphic conditions preserved in the rocks of the Napier Complex.

7 | CONCLUSIONS

1. The application of garnet–zircon partitioning arrays allows the visualization of multiple populations of

zircon against selected garnet compositions. This enables the zircon–garnet equilibrium and trends towards equilibrium to be more easily identified when unravelling the relationship between multiple zircon textures and garnet generations.

2. The bulk of the metamorphic zircon growth and recrystallization in the Napier Complex occurred in equilibrium with the peak metamorphic assemblages at >900°C.

3. A *c.* 2,850 Ma population of zircon grains was identified, consistent with earlier studies that reported a low-*P*, high-*T* magmatic/metamorphic event. Ti-in-zircon thermometry indicates that the temperature of this event was >900°C and that this event was also a regional UHT event.

4. The duration of UHT metamorphism in the Napier Complex was *c.* 135 Ma (from 2,585 to 2,450 Ma), and driven primarily by radiogenic self-heating under an orogenic plateau related to the amalgamation of Earth's first supercontinents/cratons. Temperatures were enhanced by a combination of elevated mantle temperature, the presence of a significant volume of preconditioned (previously metamorphosed) crust and the retention of HPEs in the mid-to-lower crust.

ACKNOWLEDGEMENTS

ORCID

Chris Clark http://orcid.org/0000-0001-9982-7849

REFERENCES

Alessio, K. L., Hand, M., Kelsey, D. E., Williams, M. A., Morrissey, L. J., & Barovich, K. (2018). Conservation of deep crustal heat production. *Geology*, *000*, 1–4.

Anders, E., & Grevesse, N. (1989). Abundances of the elements: Meteoritic and solar. *Geochimica et Cosmochimica Acta*, *53*(1), 197–214. https://doi.org/10.1016/0016-7037(89)90286-X

Asami, M., Suzuki, K., & Grew, E. S. (2002). Chemical Th-U-total Pb dating by electron microprobe analysis of monazite, xenotime and zircon from the Archean Napier Complex, East Antarctica:

Evidence for ultra-high-temperature metamorphism at 2400 Ma. *Precambrian Research*, *114*(3–4), 249–275. https://doi.org/10.1016/S0301-9268(01)00228-5

Baldwin, J. A., Brown, M., & Schmitz, M. D. (2007). First application of titanium-in-zircon thermometry to ultrahigh-temperature metamorphism. *Geology*, *35*(4), 295–298. https://doi.org/10.1130/G23285A.1

Bea, F. (2012). The sources of energy for crustal melting and the geochemistry of heat-producing elements. *Lithos*, *153*, 278–291. https://doi.org/10.1016/j.lithos.2012.01.017

Black, L. P. (1988). Isotopic resetting of U-Pb zircon and Rb-Sr and Sm-Nd whole-rock systems in enderby land, Antarctica: Implications for the interpretation of isotopic data from polymetamorphic and multiply deformed terrains. *Precambrian Research*, *38*(4), 355–365. https://doi.org/10.1016/0301-9268(88)90033-2

Black, L. P., James, P. R., & Harley, S. L. (1983a). Geochronology and geological evolution of metamorphic rocks in the Field Islands area, East Antarctica. *Journal of Metamorphic Geology*, *1*(4), 277–303. https://doi.org/10.1111/j.1525-1314.1983.tb00276.x

Black, L. P., James, P. R., & Harley, S. L. (1983b). The geochronology, structure and metamorphism of early Archaean rocks at Fyfe Hills, Enderby Land, Antarctica. *Precambrian Research*, *21*(3), 197–222. https://doi.org/10.1016/0301-9268(83)90041-4

Black, L. P., Sheraton, J. W., & James, P. R. (1986). Late Archaean granites of the Napier Complex, Enderby Land, Antarctica: A comparison of Rb-Sr, Sm-Nd and U-Pb isotopic systematics in a complex terrain. *Precambrian Research*, *32*(4), 343–368. https://doi.org/10.1016/0301-9268(86)90036-7

Black, L. P., Williams, I. S., & Compston, W. (1986). Four zircon ages from one rock: The history of a 3930 Ma-old granulite from Mount Sones, Enderby Land, Antarctica. *Contributions to Mineralogy and Petrology*, *94*, 427–437. https://doi.org/10.1007/BF00376336

Brown, M. (2007). Metamorphic conditions in orogenic belts: A record of secular change. *International Geology Review*, *49*(3), 193–234. https://doi.org/10.2747/0020-6814.49.3.193

Brown, M., & Johnson, T. E. (2018). Secular change in metamorphism and the onset of global plate tectonics. *American Mineralogist*, *103*, 181–196. https://doi.org/10.2138/am-2018-6166

Buick, I. S., Hermann, J., Williams, I. S., Gibson, R. L., & Rubatto, D. (2006). A SHRIMP U-Pb and LA-ICP-MS trace element study of the petrogenesis of garnet-cordierite-orthoamphibole gneisses from the Central Zone of the Limpopo Belt, South Africa. *Lithos*, *88*(1–4), 150–172.

Carson, C. J., Ague, J. J., & Coath, C. D. (2002). U–Pb geochronology from Tonagh Island, East Antarctica: Implications for the timing of ultra-high temperature metamorphism of the Napier Complex. *Precambrian Research*, *116*(3), 237–263. https://doi.org/10.1016/S0301-9268(02)00023-2

Carson, C. J., Ague, J. J., Grove, M., Coath, C. D., & Harrison, T. M. (2002). U–Pb isotopic behaviour of zircon during upper-amphibolite facies fluid infiltration in the Napier Complex, east Antarctica. *Earth and Planetary Science Letters*, *199*(3), 287–310. https://doi.org/10.1016/S0012-821X(02)00565-4

Choi, S. H., Mukasa, S. B., Andronikov, A. V., Osanai, Y., Harley, S. L., & Kelly, N. M. (2006). Lu–Hf systematics of the ultra-high temperature Napier Metamorphic Complex in Antarctica: Evidence for the early Archean differentiation of Earth's mantle. *Earth and Planetary Science Letters*, *246*(3), 305–316. https://doi.org/10.1016/j.epsl.2006.04.012

Clark, C., Collins, A. S., Santosh, M., Taylor, R., & Wade, B. P. (2009). The *P–T–t* architecture of a Gondwanan suture: REE, U-Pb and Ti-in-zircon thermometric constraints from the Palghat Cauvery shear system, South India. *Precambrian Research*, *174*(1–2), 129–144. https://doi.org/10.1016/j.precamres.2009.07.003

Clark, C., Fitzsimons, I. C. W., Healy, D., & Harley, S. L. (2011). How does the continental crust get really hot? *Elements*, *7*(4), 235–240. https://doi.org/10.2113/gselements.7.4.235

Clark, C., Healy, D., Johnson, T. E., Collins, A. S., Taylor, R. J., Santosh, M., & Timms, N. E. (2015). Hot orogens and supercontinent amalgamation: A Gondwanan example from southern India. *Gondwana Research*, *28*(4), 1310–1328. https://doi.org/10.1016/j.gr.2014.11.005

Collins, W. J. (2002). Hot orogens, tectonic switching, and creation of continental crust. *Geology*, *30*(6), 535–538. https://doi.org/10.1130/0091-7613(2002)030<0535:HOTSAC>2.0.CO;2

Cottle, J. M., Kylander-Clark, A. R., & Vrijmoed, J. C. (2012). U-Th/Pb geochronology of detrital zircon and monazite by single shot laser ablation inductively coupled plasma mass spectrometry (SS-LA-ICPMS). *Chemical Geology*, *332–333*, 136–147. https://doi.org/10.1016/j.chemgeo.2012.09.035

Dallwitz, W. B. (1968). Co-existing sapphirine and quartz in granulite from Enderby Land, Antarctica. *Nature*, *219*, 476–477. https://doi.org/10.1038/219476a0

Eggins, S. M., Rudnick, R. L., & McDonough, W. F. (1998). The composition of peridotites and their minerals: A laser-ablation ICP–MS study. *Earth and Planetary Science Letters*, *154*(1), 53–71. https://doi.org/doi: 10.1016/S0012-821X(97)00195-7

Ellis, D. J. (1980). Osumilite-sapphirine-quartz granulites from Enderby Land, Antarctica: P-T conditions of metamorphism, implications for garnet-cordierite equilibria and the evolution of the deep crust. *Contributions to Mineralogy and Petrology*, *74*(2), 201–210. https://doi.org/10.1007/BF01132005

Ellis, D. J., Sheraton, J. W., England, R. N., & Dallwitz, W. B. (1980). Osumilite-sapphirine-quartz granulites from Enderby Land Antarctica-mineral assemblages and reactions. *Contributions to Mineralogy and Petrology*, *72*, 123–143. https://doi.org/10.1007/BF00399473

Ferry, J. M., & Watson, E. B. (2007). New thermodynamic models and revised calibrations for the Ti-in-zircon and Zr-in-rutile thermometers. *Contributions to Mineralogy and Petrology*, *154*(4), 429–437. https://doi.org/10.1007/s00410-007-0201-0

Fitzsimons, I. C. W. (2016). Pan–African granulites of Madagascar and southern India: Gondwana assembly and parallels with modern Tibet. *Journal of Mineralogical and Petrological Sciences*, *111*(2), 73–88. https://doi.org/10.2465/jmps.151117

Gauthiez-Putallaz, L., Rubatto, D., & Hermann, J. (2016). Dating prograde fluid pulses during subduction by in situ U–Pb and oxygen isotope analysis. *Contributions to Mineralogy and Petrology*, *171*(2), 15. https://doi.org/10.1007/s00410-015-1226-4

Grew, E. S. (1980). Sapphirine + quartz association from Archean rocks in Enderby Land, Antarctica. *American Mineralogist*, *65*(9–10), 821–836.

Grew, E. S. (1982). Osumilite in the sapphirine-quartz terrain of Enderby Land, Antarctica: Implications for osumilite petrogenesis in the granulite facies. *American Mineralogist*, *67*, 762–787.

Grew, E. S., & Manton, W. I. (1979). Archean rocks in Antarctica: 2.5-billion-year uranium-lead ages of pegmatites in Enderby Land.

Science, *206*(4417), 443–445. https://doi.org/10.1126/science.206.4417.443

Grew, E. S., Suzuki, K., & Asami, M. (2001). CHIME ages of xenotime, monazite and zircon from beryllium pegmatites in the Napier Complex, Khmara Bay, Enderby Land, East Antarctica. *Polar Geoscience*, *14*, 99–118.

Hacker, B. R., Gnos, E., Ratschbacher, L., Grove, M., McWilliams, M., Sobolev, S. V., & Zhenhan, W. (2000). Hot and dry deep crustal xenoliths from Tibet. *Science*, *287*, 2463–2466. https://doi.org/10.1126/science.287.5462.2463

Hacker, B. R., Ritzwoller, M. H., & Xie, J. (2014). Partially melted, mica-bearing crust in Central Tibet. *Tectonics*, *33*(7), 1408–1424. https://doi.org/10.1002/2014TC003545

Harley, S. L. (1998). On the occurrence and characterization of ultra-high-temperature metamorphism. In P. J. Treloar & P. J. O'Brien (Eds.), *What drives metamorphism and metamorphic reactions?* (vol. 138, pp. 81–107). Oxford: Geological Society of London.

Harley, S. L. (2016). A matter of time: The importance of the duration of UHT metamorphism. *Journal of Mineralogical and Petrological Sciences*, *111*(2), 50–72. https://doi.org/10.2465/jmps.160128

Harley, S. L., & Black, L. P. (1987). The Archaean geological evolution of Enderby Land, Antarctica. In R. G. Park & J. Tarney (Eds.), *Evolution of the Lewisian and comparable Precambrian high grade terrains* (27th edn, pp. 285–296). Oxford: Geological Society of London.

Harley, S. L., & Black, L. P. (1997). A revised Archaean chronology for the Napier Complex, Enderby Land, from SHRIMP ion-microprobe studies. *Antarctic Science*, *9*(1), 74–91.

Harley, S. L., & Hensen, B. J. (1990). Archaean and Proterozoic high-grade terranes of East Antarctica (40-80 E): A case study of diversity in granulite metamorphism. In J. R. Ashworth & M. Brown (Eds.), *High-temperature metamorphism and crustal anatexis* (pp. 320–370). London, UK: Unwin Hyman. https://doi.org/10.1007/978-94-015-3929-6

Harley, S. L., Kinny, P. D., Snape, I., & Black, L. P. (2001). Zircon chemistry and the definition of events in Archaean granulite terrains. Paper presented at the Fourth International Archaean Symposium, Extended Abstract Volume.

Harley, S. L., & Nandakumar, V. (2016). New evidence for Palaeo-proterozoic high grade metamorphism in the Trivandrum Block, Southern India. *Precambrian Research*, *280*, 120–138. https://doi.org/10.1016/j.precamres.2016.04.018

Hermann, J., & Rubatto, D. (2003). Relating zircon and monazite domains to garnet growth zones: Age and duration of granulite facies metamorphism in the Val Malenco lower crust. *Journal of Metamorphic Geology*, *21*(9), 833–852. https://doi.org/10.1046/j.1525-1314.2003.00484.x

Hokada, T. (2001). Feldspar thermometry in ultrahigh-temperature metamorphic rocks: Evidence of crustal metamorphism attaining ~1100°C in the Archean Napier Complex, East Antarctica. *American Mineralogist*, *86*(7–8), 932–938. https://doi.org/10.2138/am-2001-0718

Hokada, T., & Harley, S. L. (2004). Zircon growth in UHT leucosome: Constraints from zircon-garnet rare earth elements (REE) relations in Napier Complex, East Antarctica. *Journal of Mineralogical and Petrological Sciences*, *99*(4), 180–190. https://doi.org/10.2465/jmps.99.180

Hokada, T., Motoyoshi, Y., Suzuki, S., Ishikawa, M., & Ishizuka, H. (2008). Geodynamic evolution of Mt. Riiser-Larsen, Napier Complex, East Antarctica, with reference to the UHT mineral associations and their reaction relations. *Geological Society, London, Special Publications*, 308(1), 253–282. https://doi.org/10.1144/sp308.13 https://doi.org/10.1144/SP308.13

Hollis, J., & Harley, S. (2002). New evidence for the peak temperatures and the near-peak pressure-temperature evolution of the Napier Complex. In J. A. Gamble, D. N. B. Skinner & S. Henrys (Eds.), *Proceedings of the 8th international symposium on antarctic earth sciences* (pp. 19–30). Wellington, New Zealand: Royal Society of New Zealand.

Horie, K., Hokada, T., Hiroi, Y., Motoyoshi, Y., & Shiraishi, K. (2012). Contrasting Archaean crustal records in western part of the Napier Complex, East Antarctica: New constraints from SHRIMP geochronology. *Gondwana Research*, 21(4), 829–837. https://doi.org/10.1016/j.gr.2011.08.013

Horton, F., Hacker, B., Kylander-Clark, A., Holder, R., & Jöns, N. (2016). Focused radiogenic heating of middle crust caused ultrahigh temperatures in southern Madagascar. *Tectonics*, 35(2), 293–314. https://doi.org/10.1002/2015TC004040

Hyndman, R. D., & Currie, C. A. (2011). Why is the North America Cordillera high? Hot backarcs, thermal isostasy and mountain belts. *Geology*, 39, 783–786. https://doi.org/10.1130/G31998.1

Hyndman, R. D., Currie, C. A., & Mazzotti, S. (2005). Subduction zone backarcs, mobile belts, and orogenic heat. *GSA Today*, 15, 4–10. https://doi.org/10.1130/1052-5173(2005)015<4:SZBMBA>2.0.CO;2

Jackson, S. E., Pearson, N. J., Griffin, W. L., & Belousova, E. A. (2004). The application of laser ablation-inductively coupled plasma-mass spectrometry to in situ U-Pb zircon geochronology. *Chemical Geology*, 211(1–2), 47–69. https://doi.org/10.1016/j.chemgeo.2004.06.017

James, P. R., & Black, L. P. (1981). A review of the structural evolution and geochronology of the Archaean Napier Complex of Enderby Land, Australian Antarctic Territory. In J. A. Glover & D. J. Groves (Eds.), *Archaean geology* (vol. 7, pp. 71–83). Perth: Special Publication, Geological Society of Australia.

Jaupart, C., Mareschal, J.-C., & Iarotsky, L. (2016). Radiogenic heat production in the continental crust. *Lithos*, 262, 398–427. https://doi.org/10.1016/j.lithos.2016.07.017

Kelly, N. M., & Harley, S. L. (2005). An integrated microtextural and chemical approach to zircon geochronology: Refining the Archaean history of the Napier Complex, east Antarctica. *Contributions to Mineralogy and Petrology*, 149(1), 57–84. https://doi.org/10.1007/s00410-004-0635-6

Kelsey, D. E., Clark, C., & Hand, M. (2008). Thermobarometric modelling of zircon and monazite growth in melt-bearing systems: Examples using model metapelitic and metapsammitic granulites. *Journal of Metamorphic Geology*, 26(2), 199–212. https://doi.org/10.1111/j.1525-1314.2007.00757.x

Kelsey, D. E., Morrissey, L. J., Hand, M., Clark, C., Tamblyn, R., Gaehl, A. A., & Marshall, S. (2017). Significance of post-peak metamorphic reaction microstructures in the ultrahigh temperature Eastern Ghats Province, India. *Journal of Metamorphic Geology*, 35(9), 1081–1109. https://doi.org/10.1111/jmg.12277

Korhonen, F. J., Clark, C., Brown, M., Bhattacharya, S., & Taylor, R. (2013). How long-lived is ultrahigh temperature (UHT) metamorphism? Constraints from zircon and monazite geochronology in the Eastern Ghats orogenic belt, India. *Precambrian Research*, 234, 322–350. https://doi.org/10.1016/j.precamres.2012.12.001

Korhonen, F. J., Clark, C., Brown, M., & Taylor, R. J. M. (2014). Taking the temperature of Earth's hottest crust. *Earth and Planetary Science Letters*, 408, 341–354. https://doi.org/10.1016/j.epsl.2014.10.028

Kotková, J., & Harley, S. L. (2010). Anatexis during high-pressure crustal metamorphism: Evidence from garnet–whole-rock REE relationships and zircon–rutile Ti–Zr thermometry in leucogranulites from the Bohemian Massif. *Journal of Petrology*, 51(10), 1967–2001. https://doi.org/10.1093/petrology/egq045

Kotková, J., Whitehouse, M., Schaltegger, U., & D'Abzac, F. X. (2016). The fate of zircon during UHT–UHP metamorphism: Isotopic (U/Pb, ^{18}O, Hf) and trace element constraints. *Journal of Metamorphic Geology*, 34(7), 719–739. https://doi.org/10.1111/jmg.12206

Kusiak, M. A., Whitehouse, M. J., Wilde, S. A., Nemchin, A. A., & Clark, C. (2013). Mobilization of radiogenic Pb in zircon revealed by ion imaging: Implications for early Earth geochronology. *Geology*, 41(3), 291–294. https://doi.org/10.1130/G33920.1

Kylander-Clark, A. R. C., & Hacker, B. R. (2014). Age and significance of felsic dikes from the UHP western gneiss region. *Tectonics*, 33(12), 2342–2360. https://doi.org/10.1002/2014TC003582

Kylander-Clark, A. R. C., Hacker, B. R., & Cottle, J. M. (2013). Laser-ablation split-stream ICP petrochronology. *Chemical Geology*, 345, 99–112. https://doi.org/10.1016/j.chemgeo.2013.02.019

Ludwig, K. R. (1998). On the treatment of concordant uranium-lead ages. *Geochimica et Cosmochimica Acta*, 62, 665–676.

MacDonald, J. M., Goodenough, K. M., Wheeler, J., Crowley, Q., Harley, S. L., Mariani, E., & Tatham, D. (2015). Temperature–time evolution of the Assynt Terrane of the Lewisian Gneiss Complex of Northwest Scotland from zircon U-Pb dating and Ti thermometry. *Precambrian Research*, 260, 55–75. https://doi.org/10.1016/j.precamres.2015.01.009

Motoyoshi, Y., Hensen, B. J., & Matsueda, H. (1990). Metastable growth of corundum adjacent to quartz in a spinel-bearing quartzite from the Archean Napier Complex, Antarctica. *Journal of Metamorphic Geology*, 8(1), 125–130. https://doi.org/10.1111/j.1525-1314.1990.tb00459.x

Nabelek, P. I., Whttington, A. G., & Hofmeister, A. M. (2010). Strain-heating as a mechanism for partial melting and UHT metamorphism in convergent orogens: Implications of temperature-dependent thermal diffusivity and rheology. *Journal of Geophysical Research*, 115, B12417. https://doi.org/10.1029/2010JB007727

Paton, C., Hellstrom, J., Paul, B., Woodhead, J., & Hergt, J. (2011). Iolite: Freeware for the visualisation and processing of mass spectrometric data. *Journal of Analytical Atomic Spectrometry*, 26(12), 2508–2518. https://doi.org/10.1039/c1ja10172b https://doi.org/10.1039/c1ja10172b

Paton, C., Woodhead, J. D., Hellstrom, J. C., Hergt, J. M., Greig, A., & Maas, R. (2010). Improved laser ablation U-Pb zircon geochronology through robust downhole fractionation correction. *Geochemistry, Geophysics, Geosystems*, 11(3), 1–36.

Pearce, N. J. G., Perkins, W. T., Westgate, J. A., Gorton, M. P., Jackson, S. E., Neal, C. R., & Chenery, S. P. (1997). A Compilation of New and Published Major and Trace Element Data for NIST SRM 610 and NIST SRM 612 Glass Reference Materials. *Geostandards Newsletter*, 21(1), 115–144. https://doi.org/10.1111/j.1751-908X.1997.tb00538.x

Piazolo, S., La Fontaine, A., Trimby, P., Harley, S. L., Yang, L., Armstrong, R. A., & Cairney, J. M. (2016). Deformation-induced

trace element redistribution in zircon revealed using atom probe tomography. *Nature Communications*, 7, 10490. https://doi.org/10.1038/ncomms10490

Pownall, J. M., Hall, R., Armstrong, R. A., & Forster, M. A. (2014). Earth's youngest known ultrahigh-temperature granulites discovered on Seram, eastern Indonesia. *Geology*, 42(4), 279–282. https://doi.org/10.1130/G35230.1

Rubatto, D. (2002). Zircon trace element geochemistry: Partitioning with garnet and the link between U-Pb ages and metamorphism. *Chemical Geology*, 184(1–2), 123–138. https://doi.org/10.1016/S0009-2541(01)00355-2

Rubatto, D. (2017). Zircon: The Metamorphic Mineral. *Reviews in Mineralogy and Geochemistry*, 83(1), 261–295.

Rubatto, D., & Hermann, J. (2003). Zircon formation during fluid circulation in eclogites (Monviso, Western Alps): Implications for Zr and Hf budget in subduction zones. *Geochimica et Cosmochimica Acta*, 67, 2173–2187. https://doi.org/10.1016/S0016-7037(02)01321-2

Rubatto, D., & Hermann, J. (2007). Experimental zircon/melt and zircon/garnet trace element partitioning and implications for the geochronology of crustal rocks. *Chemical Geology*, 241(1–2), 38–61. https://doi.org/10.1016/j.chemgeo.2007.01.027

Sandiford, M. A. (1985). The origin of retrograde shear zones in the Napier Complex: Implications for the tectonic evolution of Enderby Land, Antarctica. *Journal of Structural Geology*, 7, 477–488. https://doi.org/10.1016/0191-8141(85)90050-1

Sandiford, M. A., & Wilson, C. J. L. (1983). The geology of the Fyfe Hills - Khmara Bay region, Enderby Land. In R. L. Oliver, P. R. James & B. Jago (Eds.), *Antarctic Geoscience* (pp. 16–19). Canberra, Australia: Australian Academy of Sciences.

Schaltegger, U., Fanning, C. M., Gunther, D., Maurin, J. C., Schulmann, K., & Gebauer, D. (1999). Growth, annealing and recrystallization of zircon and preservation of monazite in high-grade metamorphism: Conventional and in-situ U-Pb isotope, cathodoluminescence and microchemical evidence. *Contributions to Mineralogy and Petrology*, 134, 186–201. https://doi.org/10.1007/s004100050478

Shaffer, M., Hacker, B. R., Ratschbacher, L., & Kylander-Clark, A. R. C. (2017). Foundering triggered by the collision of India and Asia captured in xenoliths. *Tectonics*, 36(10), 1913–1933. https://doi.org/10.1002/2017TC004704

Sheraton, J. W., Thomson, J. W., & Collerson, K. D. (1987). Mafic dyke swarms of Antarctica. *Geological Association of Canada Special Publication*, 34, 419–432.

Sheraton, J. W., Tingey, R. J., Black, L. P., Offe, L. A., & Ellis, D. J. (1987). *Geology of Enderby Land and western Kemp Land*, vol. 223. Antarctica: Bureau of Mineral Resources, Bulletin-Australia.

Shimizu, H., Tsunogae, T., & Santosh, M. (2013). Petrology and phase equilibrium modeling of sapphirine + quartz assemblage from the Napier Complex, East Antarctica: Diagnostic evidence for Neoarchean ultrahigh-temperature metamorphism. *Geoscience Frontiers*, 4(6), 655–666. https://doi.org/10.1016/j.gsf.2012.09.001

Shiraishi, K., Ellis, D. J., Fanning, C. M., Hiroi, Y., Kagami, H., & Motoyoshi, Y. (1997). Re-examination of the metamorphic and protolith ages of the Rayner Complex, Antarctica: Evidence for the Cambrian (Pan-African) regional metamorphic event. In C. A. Ricci (Ed.), *The Antarctic Region: Geological Evolution and Processes* (pp. 79–88). Siena, Italy: Terra Antarctica Publication.

Sláma, J., Košler, J., Condon, D. J., Crowley, J. L., Gerdes, A., Hanchar, J. M., . . . Whitehouse, M. J. (2008). Plešovice zircon - A new natural reference material for U-Pb and Hf isotopic microanalysis. *Chemical Geology*, 249(1-2), 1–35. https://doi.org/10.1016/j.chemgeo.2007.11.005

Stern, R. A., & Amelin, Y. (2003). Assessment of errors in SIMS zircon U-Pb geochronology using a natural zircon standard and NIST SRM 610 glass. *Chemical Geology*, 197(1–4), 111–142. https://doi.org/10.1016/S0009-2541(02)00320-0

Stern, R. A., Bodorkos, S., Kamo, S. L., Hickman, A. H., & Corfu, F. (2009). Measurement of SIMS instrumental mass fractionation of Pb isotopes during zircon dating. *Geostandards and Geoanalytical Research*, 33(2), 145–168. https://doi.org/10.1111/j.1751-908X.2009.00023.x

Štípská, P., Powell, R., Hacker, B. R., Holder, R., & Kylander-Clark, A. R. C. (2016). Uncoupled U/Pb and REE response in zircon during the transformation of eclogite to mafic and intermediate granulite (Blanský les, Bohemian Massif). *Journal of Metamorphic Geology*, 34(6), 551–572.

Suzuki, S., Arima, M., Williams, I. S., Shiraishi, K., & Kagami, H. (2006). Thermal History of UHT Metamorphism in the Napier Complex, East Antarctica: Insights from Zircon, Monazite, and Garnet Ages. *The Journal of Geology*, 114(1), 65–84. https://doi.org/10.1086/498100

Taylor, R. J. M., Clark, C., Harley, S. L., Kylander-Clark, A. R. C., Hacker, B. R., & Kinny, P. D. (2017). Interpreting granulite facies events through rare earth element partitioning arrays. *Journal of Metamorphic Geology*, 35(7), 759–775. https://doi.org/10.1111/jmg.12254

Taylor, R. J. M., Clark, C., Johnson, T. E., Santosh, M., & Collins, A. S. (2015). Unravelling the complexities in high-grade rocks using multiple techniques: The Achankovil Zone of southern India. *Contributions to Mineralogy and Petrology*, 169(5), 51. https://doi.org/10.1007/s00410-015-1147-2

Taylor, R. J. M., Harley, S. L., Hinton, R. W., Elphick, S., Clark, C., & Kelly, N. M. (2015). Experimental determination of REE partition coefficients between zircon, garnet and melt: A key to understanding high-T crustal processes. *Journal of Metamorphic Geology*, 33(3), 231–248. https://doi.org/10.1111/jmg.12118

Taylor, R. J. M., Kirkland, C. L., & Clark, C. (2016). Accessories after the facts: Constraining the timing, duration and conditions of high-temperature metamorphic processes. *Lithos*, 264, 239–257. https://doi.org/10.1016/j.lithos.2016.09.004

Tomkins, H. S., Powell, R., & Ellis, D. J. (2007). The pressure dependence of the zirconium-in-rutile thermometer. *Journal of Metamorphic Geology*, 25(6), 703–713. https://doi.org/10.1111/j.1525-1314.2007.00724.x

Viete, D. R., & Lister, G. S. (2017). On the significance of short-duration regional metamorphism. *Journal of the Geological Society*, 174(3), 377–392. https://doi.org/10.1144/jgs2016-060

Walsh, A. K., Kelsey, D. E., Kirkland, C. L., Hand, M., Smithies, R. H., Clark, C., & Howard, H. M. (2015). P–T–t evolution of a large, long-lived, ultrahigh-temperature Grenvillian belt in central Australia. *Gondwana Research*, 28(2), 531–564. https://doi.org/10.1016/j.gr.2014.05.012

Watson, E. B., & Harrison, T. M. (2005). Zircon thermometer reveals minimum melting conditions on earliest Earth. *Science*, 308 (5723), 841–844. https://doi.org/10.1126/science.1110873

Whitehouse, M. J., & Platt, J. P. (2003). Dating high-grade metamorphism - constraints from rare-earth elements in zircon and garnet. *Contributions to Mineralogy and Petrology*, 145(1), 61–74. https://doi.org/10.1007/s00410-002-0432-z

Wiedenbeck, M., Hanchar, J. M., Peck, W. H., Sylvester, P., Valley, J., Whitehouse, M., & Zheng, Y. F. (2004). Further characterisation of the 91500 zircon crystal. *Geostandards and Geoanalytical Research*, *28*(1), 9–39. https://doi.org/10.1111/j.1751-908X.2004.tb01041.x

Yakymchuk, C., Clark, C., & White, R. W. (2017). Phase Relations, Reaction Sequences and Petrochronology. *Reviews in Mineralogy and Geochemistry*, *83*(1), 13–53.

Yakymchuk, C., Kirkland, C. L., & Clark, C. (2018). Th/U ratios in metamorphic zircon. *Journal of Metamorphic Geology*, in press. https://doi.org/10.1111/jmg.12307

SUPPORTING INFORMATION

Additional supporting information may be found online in the Supporting Information section at the end of the article.

Figure S1. Individual Tera–Wasserburg concordia diagrams for all samples.

Figure S2. Spot locations for individual zircon analyses.
Table S1. U–Pb and trace element LASS data for zircon from Enderby Land.
Table S2. LA-ICP-MS garnet analyses.